Petroleum Science 23 (2026) 7456–7471

Contents lists available at ScienceDirect

Petroleum Science

journal homepage: www.keaipublishing.com/en/journals/petroleum-science

Original Paper

Core-derived microbial community similarity reveals inter-well connectivity in subsurface reservoirs: Evidence from buried-hill reservoirs in the Jiyang Depression, China

Guang-Yuan Sun [a,1], Shu-Jie Xiao [b,c,1], Yong-Ting Song [b,c], Yang Gao [b,c], Ai-Min Jin [a,*], Zhang-Hua Lou [a,*]

[a] Ocean College, Zhejiang University, Zhoushan, 316021, Zhejiang, China
[b] Research Institute of Petroleum Engineering, Shengli Oilfield, SINOPEC, Dongying, 257000, Shandong, China
[c] Key Laboratory of Microbial Enhanced Oil Recovery, SINOPEC, Dongying, 257000, Shandong, China

ARTICLE INFO

Article history:
Received 28 February 2026
Received in revised form
2 July 2026
Accepted 5 July 2026
Available online 10 July 2026

Edited by Yan-Hua Sun

Keywords:
Inter-well connectivity
Microbial ecotypes
Community similarity
Core-derived microorganisms

ABSTRACT

Inter-well connectivity in deep fractured reservoirs is critical for the efficient extraction of hydrocarbon and geothermal resources. Conventional approaches, such as chemical tracers and geophysical techniques, have generally been inadequate for delineating complex fracture networks and tracing fluid migration pathways. This study proposes a novel high-throughput biogeochemical method based on core-derived microbial similarity as a proxy to infer inter-well connectivity. This method is founded on the hypothesis that hydraulic connectivity promotes community homogenization through environmental selection and dispersal. Core samples were collected from 16 wells in the buried-hill reservoir, Jiyang Depression, China, and analyzed via 16S rRNA gene sequencing to assess microbial community similarity. The results demonstrated that the studied wells could be classified into four distinct ecotypes (Types A–D) according to community diversity, phylogenetic distance, and predicted metabolic functions. Types A and B exhibited distinct community similarity patterns, which were hypothesized to reflect contrasting intra-group hydraulic connectivity: “highly heterogeneous” (Type A) and “stable homogeneous” (Type B). These patterns were consistent with fluid dynamics inferred from seismic calibration, which were influenced by structural discontinuities. In contrast, Type C showed physical isolation and poor connectivity due to the pinch-out of reservoir sandbodies. Type D, characterized by a higher abundance of rare taxa, suggested a distinct sedimentary-diagenetic environment. Microbial data specifically responded to and integrated multiple geochemical signals, thereby translating limited geochemical variables into high-throughput “biological fingerprints” that allowed refined micro-zonation within connectivity units. This study introduced core-based microbial analysis as a reservoir assessment tool, offering a new biogeochemical perspective for characterizing connectivity in fractured reservoirs and optimizing developmental stratigraphic units.
© 2026 The Authors. Publishing services by Elsevier B.V. on behalf of KeAi Communications Co. Ltd. This is an open access article under the CC BY-NC-ND license (http://creativecommons.org/licenses/by-nc-nd/4.0/).

1. Introduction

Subsurface fracture networks serve as vital geological frameworks that govern fluid migration and energy exchange inside the Earth's crust. Their spatial connectivity has a direct impact on subsurface flow patterns, resource distribution, and geomechanical stability, making it critical for the exploitation of geological resources such as hydrocarbons and geothermal energy (Zhang et al., 2020). Thus, building trustworthy reservoir models and improving engineering techniques, such as hydraulic fracturing designs, depend on accurately defining inter-well fracture connectivity. However, inadequate resolution frequently limits the use of traditional reservoir characterization techniques, such as well logging and seismic approaches, making it challenging to directly map inter-well flow conduits (Ligtenberg, 2005). The amount of noble gas and other tracers available and their capacity to differentiate between parallel flow routes and isolated hydraulic

* Corresponding authors.
E-mail addresses: aiminjin@163.com (A.-M. Jin), iwr@zju.edu.cn (Z.-H. Lou).
Peer review under the responsibility of China University of Petroleum (Beijing).
[1] These authors contributed equally to this work and should be considered co-first authors.

https://doi.org/10.1016/j.petsci.2026.07.005
1995-8226/© 2026 The Authors. Publishing services by Elsevier B.V. on behalf of KeAi Communications Co. Ltd. This is an open access article under the CC BY-NC-ND license (http://creativecommons.org/licenses/by-nc-nd/4.0/).

units constrain the efficacy of hydrochemical and tracer-based techniques in complicated fracture networks, even if they may represent fluid movement through transport characteristics (Dahlke et al., 2015; Juliusson and Horne, 2013). Although numerical modeling provides a predictive method, it is highly dependent on precise input parameters pertaining to fracture geometry and conductivity, which introduces substantial uncertainty in real-world applications (Li et al., 2025; Yousefi et al., 2018). Given these constraints, available datasets frequently lack the multidimensional information required to accurately define the complicated connection architectures seen in fractured reservoirs. As a result, creating novel high-specificity, multidimensional characterization methods is critical to overcoming present constraints in reservoir assessments.

The subsurface provides habitat to enormous microbial biomass and phylogenetic variety, which powers essential biogeochemical processes and keeps ecosystems functioning (Kallmeyer et al., 2012; Magnabosco et al., 2018; Sinclair and Ghiorse, 1989). The dispersal of subsurface microorganisms is determined by both geological restrictions and environmental conditions. Reservoir features, such as lithology, pore structure, and permeability, determine microbial habitats and limit their migration, while also modifying environmental parameters like temperature, pressure, redox potential, and nutrient input, which impact community composition (Fredrickson and Balkwill, 2006; Hinrichs and Inagaki, 2012). For instance, tight pore geometries provide microscale heterogeneity in organic carbon bioavailability through restricting substrate accessibility and microbial trophic categories (Xiao et al., 2024). The enrichment of specialized microbial groups, such as sulfate-reducing bacteria (SRBs, e.g., *Desulfobulbaceae*) in high-sulfate conditions or iron-reducing bacteria (IRBs, e.g., *Geobacteraceae*) in iron-rich environments, serves as a bioindicator of prevailing geochemical processes (Chen et al., 2025; Okoro et al., 2014). Advances in high-throughput sequencing, particularly 16S rRNA gene amplicon sequencing, enable extensive profiling of complex underground microbiomes, revealing taxonomic makeup, functional potential, and phylogenetic structure, from which ambient geological conditions may be established (Rizzo et al., 2020; Shokralla et al., 2012). For instance, oligotrophs frequently predominate in nutrient-poor deep underground habitats, and the relative abundances of copiotrophic versus oligotrophic species reflect energy regimes and nutrient availability (Finn et al., 2017). Such microbial profiles constitute informative “biological fingerprints” that may reveal hydraulic connectivity, as similar communities are expected within the same flow unit whereas isolated compartments host distinct microbiomes. Specifically, fractures, faults, and other hydraulic pathways enable the physical dispersal of microorganisms across spatial scales, which allows otherwise isolated populations to mix, reducing β-diversity and homogenizing community composition (Ning et al., 2024; Petro et al., 2017). Additionally, fluid exchange imposes shared geochemical boundary conditions such as salinity, redox potential, and nutrient availability, which exert uniform selective pressures across the connected unit (Rizzo et al., 2020; Ning et al., 2024). Thus, community similarity emerges from the interplay of dispersal and selection, thereby offering a potential tool for mapping inter-well hydraulic connectivity between wells (Miettinen et al., 2018). Core samples offer a direct view into deep subsurface environments, retaining not only lithological, structural, and diagenetic documents, but also indigenous microorganisms connecting geological history to subsurface ecology. Even at depths of several kilometers, significant prokaryotic populations exist within crystalline and sedimentary rocks (Fredrickson and Balkwill, 2006). Core-derived microorganisms arise from long-term resident populations adhering to mineral surfaces and microfractures, as well as from organisms transported via fluids through interconnected pore networks (Lehman et al., 2001). As a result, microbial communities are closely linked to long-term geological processes such as mineral weathering and diagenesis, serving as permanent biological markers that reflect native reservoir conditions and interconnected networks (Fierer et al., 2007). Fracture networks allow for microbial mixing and homogenization within hydraulically connected structures, whereas isolated compartments produce separate communities as a result of evolutionary divergence and environmental variances. In comparison to fluid samples, which are susceptible to contamination from drilling or injection fluids, core-derived microbial communities better preserve in situ biological signals over geological timescales and provide precisely located samples that can be integrated with geochemical data at the same spatial scale (Lever et al., 2013). Although core-derived microorganisms have been examined for their involvement in biogeochemical cycles (such as sulfate reduction and methanogenesis), the use of microbial spatial distributions to estimate inter-well fracture connectivity remains unexplored. Combining high-throughput microbiological profiling with core sampling presents a potential strategy for identifying hydraulic units with high specificity.

Based on this foundation, this study aims to evaluate the feasibility of core-derived microbial community structure as a method for assessing inter-well fracture connectivity. We systematically collected core samples from wells in a target reservoir and analyzed them using high-throughput sequencing. Beyond assessing overall community similarities, we identified indicator taxa and functional groupings associated with specific environmental circumstances. Similar “ecotypes” identified by microbial profiles were employed, along with stratigraphic and well-log-seismic correlations, to predict probable fracture connections. This study addressed the following questions: (1) Are the distributions of subsurface core-derived microorganisms geographically diverse? (2) Which microbial fingerprints indicate particular environmental conditions and connectivity patterns? (3) What advantages might microbial data provide over traditional chemical and geological data in reservoir analysis? We propose that community similarity under specific geological constraints reflects the integrated effects of long-term fluid exchange and shared environmental selection. This long-term perspective offers distinct advantages for reservoir characterization, such as identifying paleo-fluid migration pathways. Compared to chemical tracers or fluid microbiome techniques, core-derived microbial analysis provides higher spatial specificity and is less susceptible to engineering-induced perturbations, which is applicable to supporting decision-making in hydrocarbon production, geothermal reservoir management, and groundwater resource characterization.

2. Materials and methods

2.1. Research region and core sampling

The target region is located inside the Chengdao–Zhuangxi buried-hill oil reservoir, which is situated in the northeastern section of the Jiyang Depression in eastern China and consists principally of the Chengdao, Zhuanghai, and Zhuangxi buried hills. This reservoir shows old topographic highs that were eventually submerged and covered by newer layers, exhibiting stacked evolution, structural variety, and reservoir heterogeneity as a result of numerous tectonic processes (including Indosinian compression, Yanshanian extension and strike-slip, and Himalayan activity). The enormous burial depth and intricate geological structure of this buried-hill system present substantial hurdles in understanding its internal fracture connectivity, which is critical for effective

utilization. The Chengdao buried-hill belt has three major fault systems, including NW-trending (Indosinian compressional thrust), NNE-trending (Yanshanian–Himalayan strike-slip), and near EW-trending (Yanshanian–Himalayan extensional). The Chengbei Fault, Chengbei-20 Paleofault, Chengbei-30 North Fault, Chengbei-30 South Fault, and Zhuangnan Fault are among the most significant. The reservoir is principally composed of Lower Paleozoic Ordovician limestone and Cambrian dolomite, covered by Mesozoic and Dongying Formation mudstones, as well as Carboniferous–Permian coal-bearing layers. Hydrocarbon source rocks are mostly sourced from the lower Es_3. Although multiple exploration and early development wells (e.g., CB7, CB8, ZG1) have been drilled in this belt, large-scale development operations such as water flooding or acid stimulation have yet to be carried out, leaving the natural hydraulic connectivity among wells unclear. To investigate inter-well connectivity, core samples were taken from production wells in the Chengbei belt that had not been extensively developed. Fig. S1 showed the geographical distributions of the sampled wells. In addition, the CHE4 well from the developed CHE-44 block in Wudi County, Shandong Province (drilled in 1993 to a depth of 2744 m) was used to examine geological conditions similar to those in the buried-hill area.

Core samples from numerous wells in the Chengbei belt were collected from the Shengli Oilfield Core Repository. Seventeen wells were selected to represent the major geological heterogeneity of the buried-hill system, including lithologies (Archean granite, Cambrian dolomite, and Ordovician limestone) and burial depths ranging from 1400 to 5000 m. Based on well log and geological data, fresh and minimally contaminated representative core plugs obtained via sealed coring were chosen from the target intervals of each well. Selected samples were promptly packed in sterile aluminum foil pouches and transported to the laboratory under refrigeration (4 °C) within 24 h to minimize exogenous microbial contamination during transit. The outer 5–10 mm surface of each core was aseptically removed in a laminar flow hood after UV sterilization, leaving approximately 10 g of interior material. The inner core was then crushed into small fragments and pulverized to 200 mesh (63 μm) to fully liberate adhered microbes. This surface-decontamination method effectively reduced drilling fluid contamination in interior core material once the outer layers are removed (Kieft et al., 2008; Lever et al., 2006; Westmeijer et al., 2023). All tools were flame-sterilized between samples, and the laminar flow hood was decontaminated with UV light and 70% ethanol before each use. Sterile gloves and face masks were worn throughout processing. Replicate core plugs were processed in separate batches to minimize cross-contamination, and a blank core (sterile soil) was included as a procedural control. Archived drilling mud samples were unavailable for sequencing, as coring operations preceded this study. The resulting core powder was deposited in sterile centrifuge tubes; a portion was utilized for subsequent genomic DNA extraction, while the remainder was stored at −80 °C for future analysis.

2.2. Hydrochemical analysis

Hydrochemical data, including total dissolved solids (TDS), Na^+, K^+, Ca^{2+}, Mg^{2+}, Cl^-, SO_4^{2-}, and HCO_3^-, were obtained from original formation fluids collected during drilling and used to characterize the in-situ geochemical background of each well. Anion and cation concentrations were analyzed using ion chromatography (DIONEX ICS-1000, USA) (Campos et al., 2020). A Shim-pack IC-A3 column was used for cations (Na^+, K^+, Ca^{2+}, Mg^{2+}), and a Shim-pack IC-C3 column was used for anions (Cl^-, SO_4^{2-}). Bicarbonate (HCO_3^-) was determined by hydrochloric acid titration. TDS was calculated as the sum of the measured ion concentrations.

2.3. DNA extraction and high-throughput sequencing

Total genomic DNA was extracted from 0.5 g of core powder using the ALFA Soil DNA Extraction Kit according to the manufacturer's instructions. The concentration and quality of the DNA were measured with a Nanodrop® ND-2000 UV-Vis spectrophotometer (Thermo Scientific, Wilmington, DE, USA) to ensure suitability for sequencing. Extraction blanks (sterile soil) and PCR negatives (no template DNA) were processed alongside the samples, and both types of negative controls showed no detectable amplification on agarose gels. The V3–V4 hypervariable region of the bacterial 16S rRNA gene was amplified using primer pairs 338F (5′-ACTCCTACGGGAGGCAGCA-3′) and 806R (5′-GGACTACHVGGG TWTCTAAT-3′) (Cui et al., 2017). The V4–V5 region of the archaeal 16S rRNA gene was amplified using primers Arch519F (5′-CA GCCGCCGCGGTAA-3′) and Arch915R (5′-GTGCTCCCCCGCCAA TTCCT-3′) (Yang et al., 2016). The 50 μL PCR mixture contained 25 μL Takara 2× Premix Taq, 1 μL each of forward and reverse primers (10 μmol/L), 1 μL template DNA (about 50 ng), 1 μL bovine serum albumin (BSA, 2 ng/μL), and 21 μL deionized water. PCR reaction protocols were as follows: initial denaturation at 94 °C for 5 min; 30 cycles of 94 °C for 30 s, 52 °C for 30 s, and 72 °C for 30 s; final extension at 72 °C for 10 min; and hold at 4 °C.

PCR products were analyzed using GeneTools Analysis Software (Version 4.03.05.0, SynGene) and purified using the E.Z.N.A.® Gel Extraction Kit (Omega, USA). Fragment length and concentration were verified. Samples showing a dominant band within the expected size range (e.g., 460–480 bp for the 16S V3–V4 region) were selected for library preparation. Purified amplicons were sequenced on an Illumina NovaSeq 6000 platform at Magigene Biotechnology Co., Ltd. (Guangzhou, China).

2.4. Bioinformatics analysis

Raw 16S rRNA sequences were processed for quality control and clustering on the Galaxy platform (Galaxy Version 1.0.0) (Feng et al., 2017). Briefly, barcodes and primers were trimmed using Fastp (Version 0.14.1) and ccs (Version 3.4.1). Paired-end reads were merged with Usearch (Version 10.0.240), requiring a minimum overlap of 16 bp and a maximum mismatch rate of 0.25. Low-quality sequences shorter than 220 bp or containing ambiguous bases (N) were filtered out using Btrim. Operational taxonomic units (OTUs) were clustered at 97% similarity using UPARSE, and an OTU table was generated. Taxonomic assignment was performed using the SILVA database and the RDP Classifier (Version 2.14).

Based on the resampled OTU table and taxonomic annotations, alpha diversity (α-diversity) indices (Chao, Shannon), beta diversity metrics (Bray–Curtis, UniFrac), and relative abundances at different taxonomic levels were calculated. Principal coordinate analysis (PCoA) was performed using Bray–Curtis distances, and sample distances were computed based on UniFrac. Functional prediction of prokaryotic communities was conducted using PICRUSt2 on the Galaxy platform (Caicedo et al., 2020). Two distance matrices were constructed for ecotype classification: bacterial Bray–Curtis distances based on relative abundances and PICRUSt2-predicted KEGG pathway abundances. These two matrices were normalized and integrated using an equal-weighting method (weights: 0.5 for community structures and 0.5 for functional profiles). PCoA was then performed on the integrated distance matrix, and the first three principal coordinates (cumulative explanatory variance >50%) were retained. Hierarchical clustering using Ward's linkage was applied to these coordinates to assign samples to ecotypes. Cluster stability was assessed via bootstrap resampling (1000 iterations). Samples with bootstrap values below 50% were considered unstable and excluded from the

integrated classification, whereas wells with bootstrap support of 70% or higher were retained as core ecotypes (Felsenstein, 1985; Soltis and Soltis, 2003). The multiple response permutation procedure (MRPP) was then used to evaluate differences in microbial community structures among ecotypes. Linear discriminant analysis effect size (LEfSe) was performed via the online tool (https://www.omicstudio.cn/tool/60), with Kruskal–Wallis and Wilcoxon test thresholds set at 0.05, and LDA score filters set at 3.8 for bacteria and 3.0 for archaea, to identify taxa with significant differential abundance across groups. The β-nearest taxon index (β-NTI) was calculated using the NST, picante, and ape packages in R (Version 4.0.5). |β-NTI| > 2 indicates that deterministic processes dominate community assembly, whereas |β-NTI| < 2 suggests stochastic processes prevail (Stegen et al., 2013; Zhou and Ning, 2017). Microbial interaction networks were constructed based on random matrix theory (RMT) using the MENA platform (http://ieg4.rccc.ou.edu/mena/main.cgi), and topological properties were analyzed (Deng et al., 2012). Network visualization was performed with Gephi (Version 0.10.1). All raw sequencing data were deposited in the Science Data Bank (ScienceDB) under dataset: https://doi.org/10.57760/sciencedb.34646.

2.5. Geological structure and stratigraphic correlation

The seismic data were acquired using artificial seismic sources (vibrator sources) and reflected signals from subsurface strata were processed using standard seismic imaging workflows. Key seismic markers, including continuous, regionally traceable strong reflection waves, were used to generate the structural graph. Logging data were obtained by lowering logging equipment into a borehole to continuously measure the physical properties of the strata along the wellbore. The vertical resolution of the seismic data in this study area was approximately 25 m, which is suitable for regional structural trend analysis. Well logging data, with the explanation accuracy of 0.125 m, were used to precisely delineate stratums within the constraints of the structural interpretation, thereby assessing reservoir connectivity. Synthetic seismograms were generated using acoustic and density log data. By iteratively adjusting wavelets and time-depth relationships, geological horizons were accurately calibrated to the seismic time domain. These marker horizons were tracked and closed in 3D space to establish a unified stratigraphic–structural framework, enabling precise inter-well stratigraphic correlation (Miall, 1995; Mitchum and Vail, 1977). The seismic profiles and well logging curves were provided by the Logging Company of Shengli Oilfield Engineering Co., Ltd., SINOPEC. Well numbers were replaced with random numbers to avoid interference from location information during the analysis.

2.6. Statistical analysis

Mean values and standard deviations of hydrochemical and microbial properties were calculated using Excel and IBM SPSS (SPSS Inc., Chicago, IL). One-way analysis of variance (ANOVA), followed by least significant difference (LSD) post-hoc tests, was performed using the agricolae package in R to assess significant differences among groups. The Benjamini–Hochberg false discovery rate (FDR) correction was applied to control the expected proportion of false positives. Adjusted q-values less than 0.05 were considered statistically significant. Basic graphs (bar charts, box plots) were generated with Origin 2024 and GraphPad Prism 10. Functional heatmaps and correlation plots were visualized using the pheatmap and ggplot2 packages in R. Microbial community similarity across different combinations of lithology and ecotypes was calculated using the Bray–Curtis distance using the "vegdist" function of the vegan package in R. Mantel tests examining the influence of environmental factors on microbial communities were conducted using the linkET, tidyverse, and dplyr packages in R. Structural equation modeling (SEM) was performed with Amos 26.

3. Results

3.1. Salinity and ionic composition

The analyzed samples exhibited considerable heterogeneity in TDS and ion concentrations, with variations correlating to stratigraphic position and burial depth, as shown in Table 1. TDS values ranged widely from 10,553 to 43,700 mg/L, generally increasing with greater geological age and depth. Formation fluids from deep Archean strata consistently displayed TDS values exceeding 43,200 mg/L, indicative of long-term fluid concentration and intense water–rock interaction in an ancient, confined environment. The ionic composition was dominated by Na^+, K^+, and Cl^-, whose concentrations showed a co-varying trend and peaked in Archean samples, reflecting pronounced evaporative concentration and subsequent isolation. Notably, distinct ionic patterns were observed across different formations. Certain Lower Paleozoic samples (e.g., CB3, ZG1, CB5) were characterized by elevated levels of Ca^{2+} (>1600 mg/L), Mg^{2+} (>1180 mg/L), and HCO_3^- (>200 mg/L), suggesting a fluid environment influenced by carbonate dissolution and active anaerobic microbial processes such as methanogenesis. Although Archean samples exhibited high

Table 1
Total mineralization and major ion concentrations of wells.

Wells	TDS, mg/L	$Na^+ + K^+$, mg/L	Ca^{2+}, mg/L	Mg^{2+}, mg/L	Cl^-, mg/L	SO_4^{2-}, mg/L	HCO_3^-, mg/L
CB1	19,326	6510	485	323	11,402	1165	167
L4	10,553	4468	813	207	5517	741	1532
CB2	22,500	8200	850	310	12,000	1150	2100
CB3	25,800	8900	1600	720	14,500	1080	2700
ZG1	32,400	10,800	1950	860	6200	1220	2950
CB4	41,500	7500	920	430	8600	650	3200
ZG2	46,500	11,200	350	150	12,100	1180	80
CB5	23,200	8300	1650	700	11,800	790	2600
ZH2	23,900	8400	780	290	13,600	720	2000
ZGX	15,200	4600	250	105	5400	520	1050
CB6	43,200	14,290	266	131	18,734	1250	2094
CB7	43,300	16,044	333	241	21,855	1291	4196
ZG4	43,593	10,560	416	181	20,113	1040	3800
ZG5	43,700	15,840	332	179	20,210	1250	7108
CHE4	23,000	8250	1630	690	11,750	720	2580

salinity, they contained relatively low concentrations of Ca^{2+} and Mg^{2+} coupled with high HCO_3^- values, potentially linked to water–rock reactions like dolomitization. Sulfate (SO_4^{2-}) concentrations were uniformly low across all samples (520–1291 mg/L) and showed no clear stratigraphic correlation, pointing to a strongly reducing environment where sulfate reduction has proceeded to near completion. These hydrochemical and ionic profiles provide a foundational context for interpreting the observed differentiation in microbial community structure and function.

3.2. Microbial community composition analysis

Clustering analysis of core-derived microbial samples from the buried-hill reservoir yielded 5311 bacterial and 65 archaeal operational taxonomic units (OTUs). Rarefaction curves indicated that the current sequencing depth sufficiently covered the majority of microbial species present (Fig. S2). Ecotypes were delineated based on community structures and functional pathways. Bootstrap resampling (1000 iterations) confirmed cluster stability, with over 70% assignment confidence for wells assigned to core ecotypes and samples with bootstrap values below 50% were excluded from the core ecotypes. Structural equation modeling (SEM) was further employed to characterize the possible correlations among connectivity (hereafter inferred from microbial ecotypes unless stated otherwise), hydrochemical parameters, and stratigraphic depth. The SEM model exhibited acceptable fits with chi-square = 2.541, df = 3, p = 0.468, CFI = 0.944, RMSEA = 0.001, and SRMR = 0.037, which met conventional thresholds for model fit (CFI > 0.90, RMSEA < 0.08, SRMR < 0.08), indicating that the hypothesized relationships among stratum, hydrochemistry, and microbial similarity were consistent with the observed data.

3.2.1. Bacterial community composition and ecotype classification

A systematic analysis of bacterial community structure and functional potential was conducted based on 16S rRNA gene sequencing data from core samples of 16 study wells and the CHE4 well. β-diversity analysis using Bray–Curtis distances initially segregated all samples into three clusters (Fig. 1(c)). However, several samples were positioned distantly from their respective cluster centroids. The abundances of metabolic pathways predicted by PICRUSt2 revealed a clear bipartite clustering of samples into high- and low-metabolism groups (Fig. 1(d)). Specifically, the high-metabolism group showed greater relative abundances of pathways related to carbon metabolism, fatty acid metabolism, and the TCA cycle, whereas these pathways were less abundant in the low-metabolism group. Beyond core metabolism, pathways associated with genetic information processing and environmental response were also less abundant in the high-metabolism group (Fig. S3), indicating the decisive role of nutrient availability in shaping microbial community divergence. Notably, nine samples from species cluster I were distributed across both high- and low-metabolism groups, while six samples from cluster II were almost exclusively within the high-metabolism group (except ZG3). Samples CB5 and CHE4 from species cluster III belonged to the high- and low-metabolism groups, respectively, possibly indicating functional divergence affected by environmental conditions in hydraulically isolated compartments. Functional classification showed a strong correlation with depth. All four wells shallower than 3200 m were classified as high-metabolism, whereas wells deeper than 5000 m were low-metabolism. In particular, the metabolic functions in ZH2, ZG1, and ZG3 appeared to be either activated or suppressed due to specific geological constraints. UniFrac distance analysis further elucidated phylogenetic relationships among samples (Fig. 1). Wells CB4, CB5, L4, and

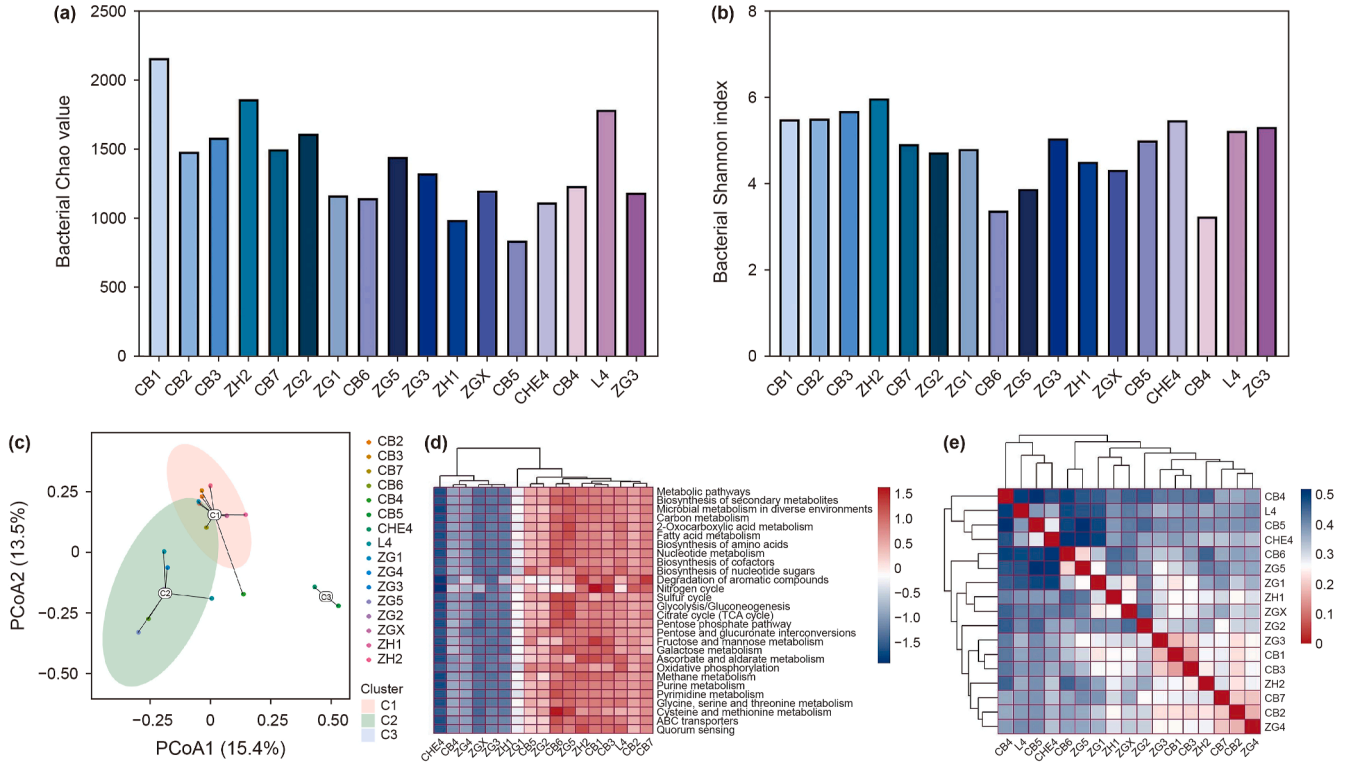


Fig. 1. The diversity, metabolic activity, and evolutionary distance of sequenced microbial communities. (**a**) Bacterial α-diversity indicated by Chao value. (**b**) Bacterial α-diversity indicated by Shannon index. (**c**) The PCoA result of bacterial community structure in 16 sequenced core samples. (**d**) Relative abundances of metabolic associated functional pathways of bacterial communities predicted by PICRUSt2. (**e**) The UniFrac distance matrix of bacterial communities.

CHE4 formed distinct, distant branches, suggesting a lack of connection with the main phylogenetic group. The close phylogenetic affinity and similar community structure between CB5 and CHE4 reaffirmed their environmental similarity. Within the high-metabolism group, CB6 and ZG5 were more closely related to each other and showed distance from other functionally similar wells. CB1, CB3, and ZH2 occupied central positions within the high-metabolism group, potentially representing active geological units supplying nutrients to other connected wells. In the low-metabolism group, ZH1 and ZGX showed closer phylogenetic relatedness.

Consequently, based on the divergence in bacterial community structure and predicted function, core-derived microbial communities were classified into four putative ecotypes (Types A–D) using the hierarchical clustering and bootstrap resampling (Table S1). Type A, characterized by high microbial diversity and metabolic activity, included CB1, CB2, CB3, ZH2, and CB7. Type B, which also exhibited high metabolic activity but relatively low biodiversity, comprised ZG2, ZG1, CB6, and ZG5. Type C, with a community structure similar to Type A, showed significantly lower metabolic activity and included ZG4, ZH1, and ZGX. Type D consisted of two wells (CB5 and CHE4) that exhibited a distinct difference from the communities of other ecotypes. CB4, L4, and ZG3 were considered unconnected to these four ecotypes, as their bootstrap probabilities were below 50% (Fig. 2(a)). Principal component analysis (PCA) confirmed significant differentiation in community structure among ecotypes, suggesting that Types A and B likely represent distinct depositional environments (Fig. 2(b)). Analysis of OTU distribution revealed that Type A (represented by CB1) harbored a greater number of species than Type B (ZG2), with some species overlap. Type C (ZG4) shared many species with Type A, while Type D contained the highest number of unique species (Fig. 2(c)). Shannon index analysis indicated significant differences in species richness and evenness among samples (Fig. 1(a) and (b)). Bacterial α-diversity was higher in Types A, C, and D compared to Type B, within which CB6 and ZG5 exhibited similarly low diversity indices (3.37–3.87).

MRPP analysis further validated the ecotype classification (observed delta = 0.690, expected delta = 0.766, $A = 0.109$, $p < 0.001$), indicating significant within-group similarity (Table S2). Pairwise comparisons revealed significant differences ($p < 0.05$) between Types A and B (delta = 0.67, $p < 0.01$), Types B and C (delta = 0.71, $p < 0.05$), and Types A and D (delta = 0.67, $p < 0.05$), confirming that Type C shared structural similarity with Type A but was functionally distinct. The observed delta and p values demonstrated that the sample size ($n = 17$) was sufficient to detect the observed effect sizes. To further quantitatively examine the driving effects of shared lithology on microbial similarity, a pairwise comparison based on Bray–Curtis distances and lithology data from well logs was performed. Wells were grouped into three categories defined by microbial ecotypes and lithology similarity: (1) same ecotype and sandstone lithology (Type A or B internal pairs); (2) different ecotype but same lithology (Type A and B, Type C internal pairs, and CB5 and CHE4); and (3) different ecotype and lithology. Results showed that community similarity in wells with the same ecotype and sandstone lithology (0.63) was significantly higher than in wells with only the same lithology (0.56) or with different lithology (0.41), indicating that the hydraulic connectivity (hypothesized by microbial ecotypes) was most closely associated with microbial convergence ($p < 0.05$, Fig. S4). Bacterial community structure and biomarker taxa also demonstrated clear differentiation among ecotypes (Fig. 3). At the class level, the

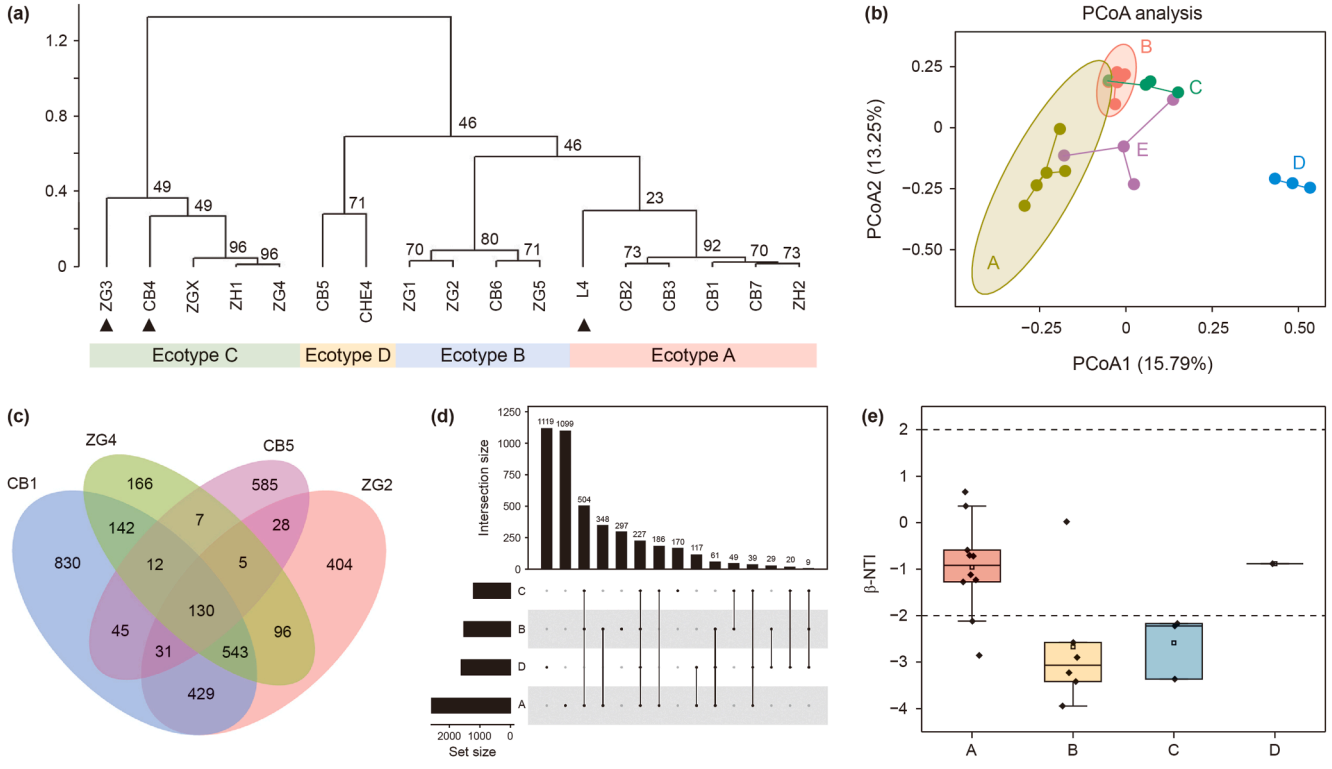


Fig. 2. The classification, biodiversity, and assembly of microbial ecotypes. (**a**) Identification of distinct core-derived microbiome ecotypes using the hierarchical clustering method. Numbers indicate bootstrap probabilities as percentages, and triangles represent samples with relatively low classification credibility that do not belong to ecotypes A–C. (**b**) PCoA analysis of microbial ecotypes based on Bray–Curtis dissimilarity. (**c**) Shared and unique OTU distributions for each ecotype-specific well. (**d**) Biomarker distribution patterns of four ecotypes revealed by an upset diagram. (**e**) Differentiation of the β-NTI index among microbial ecotypes. Values of |β-NTI| > 2 indicate deterministic assembly processes, whereas values of |β-NTI| < 2 indicate stochastic processes.

dominant taxa in Types A, B, and C were Bacilli, Alphaproteobacteria, Actinobacteria, and Gammaproteobacteria, accounting for over 65% of relative abundances (Fig. 3(a)). Bacilli were most abundant in Type B, particularly in CB6 and ZG5 (50.1%–63.7%). Type C was characterized by a higher proportion of Actinobacteria, reaching up to 48.8% in ZGX. The ratio of copiotrophic (Bacilli and Gammaproteobacteria) to oligotrophic bacteria (Alphaproteobacteria and Actinobacteria) was calculated. Results showed that copiotrophs were more prevalent in Type A (25.4%–47.2%) and Type B (37.4%–75.9%), whereas oligotrophs dominated in Type C (36.3%–62.6%). The copiotroph/oligotroph (c/o) ratio was significantly higher in Type B than in other groups ($p < 0.05$; Fig. 3(e)), indicating a copiotrophic metabolic regime. Type C exhibited the lowest c/o ratio. Type A, with a more even distribution of dominant taxa, was likely associated with a mixed trophic strategy, as its c/o was not significantly higher than that of Type C ($p > 0.05$). Type D harbored the highest proportion of rare taxa, with the dominant classes Alphaproteobacteria and Betaproteobacteria constituting only 36.3%–42.4%. At the genus level, Type A was enriched with genera capable of degrading a broad spectrum of organic compounds, including *Planococcus* (complex organic matter) and *Sphingomonas* (aromatic compounds). Type B

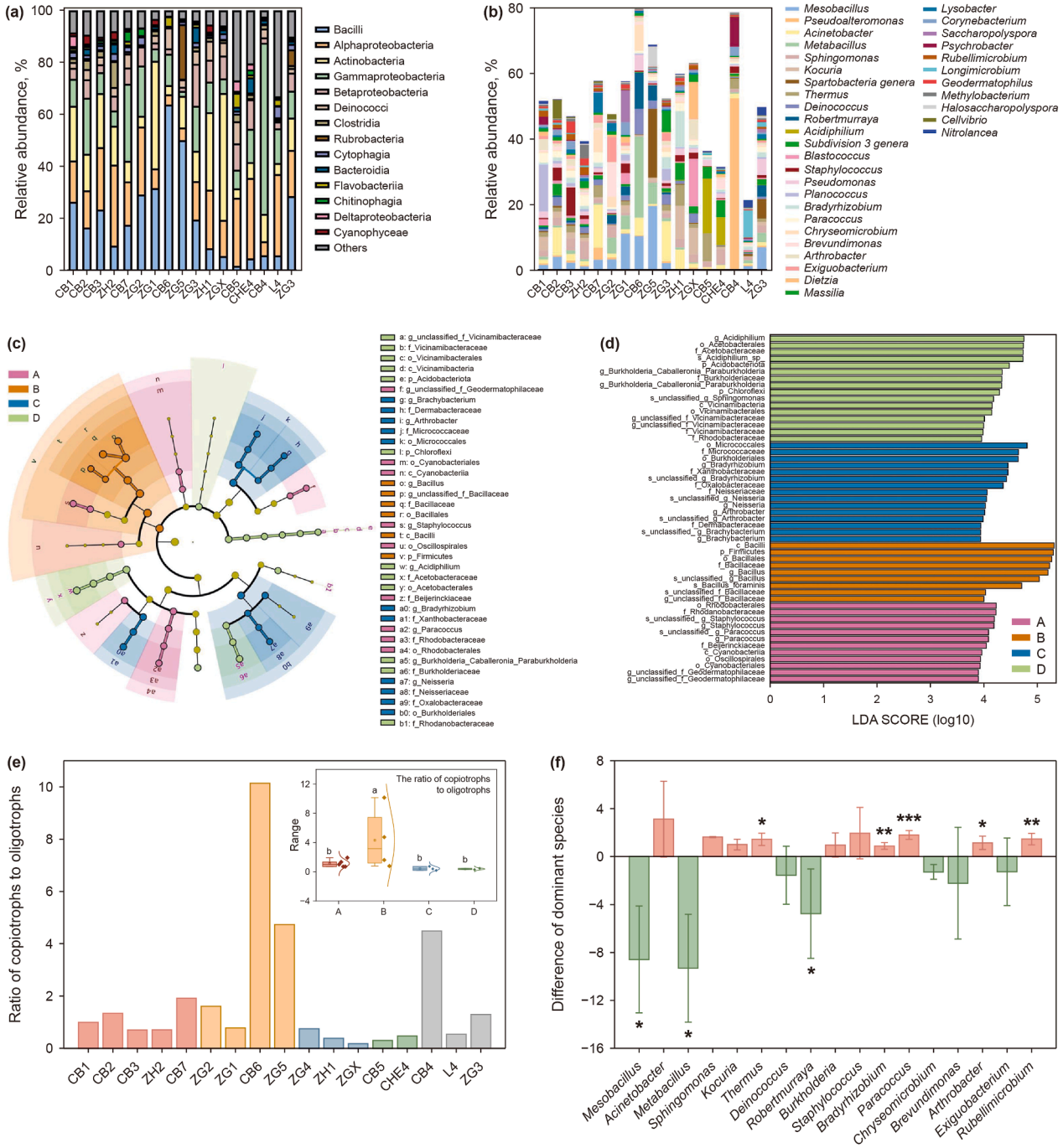


Fig. 3. Species distribution characteristics of microbial ecotypes. (**a**, **b**) Dominant bacterial species at the class and gene levels, respectively. (**c**, **d**) Biomarkers of each ecotype revealed by LEfSe cladogram and bar chart, respectively. (**e**) The ratio of copiotrophic to oligotrophic bacteria of ecotypes. (**f**) Significant differences in dominant bacterial genera between Types A and B (LSD, $p < 0.05$).

was dominated by distinct genera such as *Mesobacillus* and *Metabacillus*, which are associated with environmental stress response. Type C was enriched with *Kocuria* and *Bradyrhizobium*, indicative of oligotrophic, halotolerant, and potentially cold-adapted environments. Type D was characterized by genera such as *Acidiphilium* and *Thermus*, reflecting extreme acidic conditions and localized thermal sources (Fig. 3(b)). Linear discriminant analysis effect size (LEfSe) analysis (LDA > 3.8, Kruskal–Wallis $p < 0.05$) further highlighted distinct taxonomic markers for each ecotype, providing independent validation of the classification (Fig. 3(c)). Type A was marked by the organic degrader *Paracoccus*; Type B by *Mesobacillus* and *Halosaccharopolyspora*; Type C by *Brachybacterium*, *Arthrobacter*, and *Neisseria*; and Type D by *Gp6*, *Acidiphilium*, and *Prosthecobacter*.

Furthermore, the assembly mechanisms of bacterial communities differed significantly among ecotypes. The β-NTI analysis revealed that community assembly in Types A and D was primarily associated with stochastic processes, specifically dispersal limitation, rather than strong environmental selection ($|\beta\text{-NTI}| \leq 2$, Figs. 2(e) and S5). This likely results from significant environmental heterogeneity within these hydraulically connected units, which weakens the homogenizing effect of selection. In contrast, deterministic processes, particularly homogeneous selection, dominated in Types B and C, leading to community convergence and lower diversity within their highly uniform environments. In summary, based on bacterial community structure and functional similarity, core samples were classified into four ecotypes, which may represent distinct patterns of inter-well connectivity. Types A and B exhibited relatively dynamic and uniform community compositions under differing environmental conditions and nutrient inputs, respectively, potentially indicating corresponding connectivity patterns. Type C represented an oligotrophic, relatively isolated compartment, which might have low connectivity. Type D comprised two wells with unique geological environments. Given the block distance, no geological connectivity existed in Type D; nevertheless, the highly similar community composition indicated a shared depositional environment.

3.2.2. Archaeal community composition and environmental variability

A systematic analysis of subsurface archaeal distribution was conducted based on 16S rRNA gene sequencing data. Archaeal α-diversity was generally lower than bacterial diversity, with Shannon indices ranging from 0.85 (ZG2) to 2.38 (CB1). This metric showed no direct correspondence with the bacterial-defined ecotypes, suggesting that archaeal communities are associated with distinct ecological processes. β-diversity analysis using PCoA based on Euclidean distances partitioned archaeal communities into three relatively distinct clusters. This grouping did not fully overlap with the four bacterial ecotypes (A–D), revealing that different microbial domains respond to environmental filters at varying scales (Table S3).

LEfSe analysis indicated that core-derived archaeal communities were functionally stratified into three broad guilds: halophiles, ammonia oxidizers, and methanogens (Fig. S6). The halophilic guild was dominated by the phylum Halobacterota (class Halobacteria), constituting over 75% relative abundance, and was enriched with genera such as *Halococcus* and *Halalkalicoccus*. Samples in this guild (e.g., CB1, CB7, ZG2, ZG5, ZG4) belonged to bacterial ecotypes A and B (Fig. S7). Although bacterial indicators suggested these wells form separate hydraulic networks, the presence of halophilic archaea indicated that high salinity acted as a selective pressure within each group (TDS > 20,000 mg/L). The ammonia-oxidizing guild was dominated by nitrifying archaea from the phylum Crenarchaeota (class Nitrososphaeria, family Nitrosopumilaceae; LDA > 4.5). Samples in this guild (including CB6, ZH2, ZGX) spanned ecotypes A, B, and C, and contained a substantial proportion of unclassified rare taxa. This suggests that ammonia oxidation is a key process occurring in nitrogen-rich chemical microenvironments across different connectivity units, and that nitrogen availability is widespread and independent of connectivity strength. The methanogenic guild comprised samples where methanogenic archaea (e.g., *Methanobacterium*, *Methanobrevibacter*, and *Bathyarchaeia*) were dominant (including ZG1, CB5, and CHE4), co-occurring with elevated HCO_3^- concentrations (>2500 mg/L). Notably, CB5 and CHE4 (both Type D) were dominated by *Haloarcula* and *Methanobacterium*, respectively, and clustered more closely with CB3 and ZG1. ZG1 in Type B exhibited a strong methanogenic signal, implying the presence of a distinct, active methanogenic niche within the unit. PICRUSt2 functional prediction for archaea indicated that metabolic, genetic information processing, and signaling pathway abundances were higher in ZG2, ZG1, and CB4 compared to other wells (Fig. S8), supporting the hypothesis that ZG1 occupies an interface between high-salinity and ammonia-oxidizing/methanogenic niches within Type B. This mapping demonstrated that while hypothetical connectivity units shared broad environmental filters (e.g., high salinity in Types A and B), local biogeochemical variability within units could still drive domain-specific guild distributions. In summary, the distribution patterns of core-derived archaeal communities provide crucial supplementary biogeochemical indicators to infer microenvironmental conditions (e.g., salinity, nitrogen availability, methanogenic activity) within each ecotype. Salinity and nitrogen input may act as environmental filters, creating heterogeneity within physically connected networks, which can be revealed by archaeal bioindicators.

3.3. Inter-well stratigraphic correlation based on well-seismic calibration

High-resolution well-seismic calibration, utilizing regionally continuous reflection events from the weathered crust at the reservoir top and internal stable strata, enabled precise inter-well stratigraphic correlation and structural analysis. This provided geological evidence and a causal framework for the connectivity identification based on microbial ecotypes (A, B, and C). Based on the logging data of each well and logging interpretation conclusions, the strata in this study area were carefully compared and divided using the cycle correlation method. Above the Shahejie (Es) Formation, the baseline of the spontaneous potential (SP) curve gradually shifted; upon entering the Shahejie Formation, the baseline shift amplitude decreased, and the SP curve showed obvious negative anomalies. The curve shapes were mainly bell- and box-shaped, reflecting the great physical properties and connectivity of the reservoir.

For Type A (CB1, CB2, CB3, CB7, ZH2), the seismic profile and logging curves revealed that these wells were situated within the same buried-hill structural trend, where the reservoir exhibited lateral continuity, fulfilling the basic geological prerequisites for fluid migration and exchange (Figs. 4 and S9). However, this structural belt had experienced intense tectonic activity, resulting in a maximum vertical throw of approximately 2200 m and formation dip up to 18°. This substantial topographic relief had created heterogeneous paleotopography and fracture development patterns, leading to significant differences in fluid potential. Coupled with the geothermal gradient causing considerable temperature variations, these factors shaped more complex fluid migration pathways and habitat conditions. This geological setting explained the high environmental heterogeneity observed in Type A, which promoted mixing of fluids from different sources and

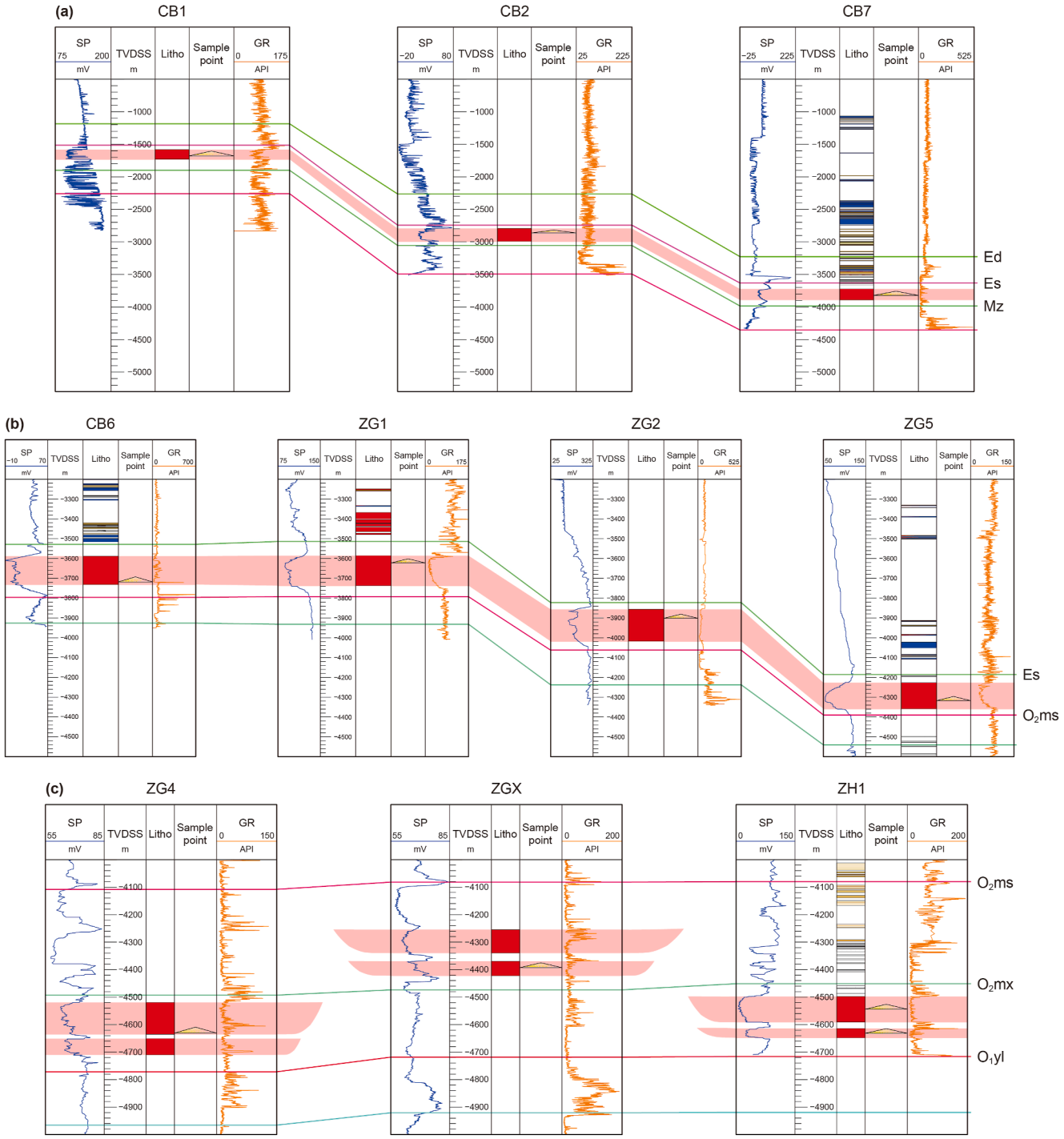


Fig. 4. Stratigraphic correlation analysis based on well calibration. (**a**) Type A; (**b**) Type B; (**c**) Type C.

nutrient transport, thereby supporting higher microbial diversity and functional divergence.

Type B (CB6, ZG5, ZG1, ZG2) was found to reside within a structurally stable block characterized by gentle relief (Fig. 4(b)). The structural throw here was limited (about 600 m) with a low formation dip angle of 2.1°. This subdued topography indicated slower inter-layer fluid movement and a stable hydraulic system, less prone to strong external fluid interference, providing favorable conditions for connectivity. These stable geological conditions provided a long-term, consistent habitat for microbial communities, leading to the enrichment of specific functional groups and a more uniform niche differentiation. Seismic data indicated that wells within Types A and B were located in continuous structural blocks without evident barriers, which was a necessary condition for hydraulic connectivity.

Conversely, well-seismic calibration for Type C (ZG4, ZGX, ZH1) showed that although the three wells were located within Middle Ordovician sedimentary strata of similar depositional environment, detailed reservoir correlation identified a pinch-out of the target sandstone bodies (Fig. 4(c)). The O_2ms formation in ZGX consisted entirely of mudstone over a long well section, whereas ZG4 and ZH1 consisted of sandstone. The sandstone bodies in ZG4

and ZH1 were separated by the mudstone in ZGX. This meant the main reservoir and fluid conduit sands thinned out and terminate laterally, creating a physical barrier that effectively isolates fluid communication between the wells. This key geological evidence confirmed the hypothesis of poor overall connectivity for Type C. Reservoir pinch-out led to the formation of relatively closed fluid systems in each well, restricting the exchange of nutrients and microorganisms, contributing to the observed lower microbial diversity and functional pathway abundances. These geological data provided foundational evidence for linking subsurface microbial ecosystems to the macro-scale geological framework.

4. Discussion

4.1. Construction of bacterial-archaeal indicators and inter-well connectivity assessment

Microbial dispersion in the subsurface demonstrated great geographic variation, driven by local geological history, hydrological conditions, and micro-environmental parameters such as redox status and nutrient availability (Fredrickson and Balkwill, 2006; Magnabosco et al., 2018; Wu et al., 2025). DNA yields from core samples ranged from 500 to 1500 ng/g of core powder, and the results showed substantial heterogeneity in microbial distributions within the deep subsurface of the Chengbei buried-hill belt. Firstly, bacterial community composition and function diverged significantly across both vertical (stratigraphic) and lateral (spatial) scales. Well pairs with minor spatial separation, such as ZG1 and ZG4 (about 200 m horizontal distance), CB4 and CB5 (about 190 m vertical), and ZG3 and ZG5 (about 143 m vertical), exhibited distinct microbial profiles (Tables 2 and 3). Conversely, wells from different stratigraphic horizons, such as ZH2 (3624 m), CB7 (3776 m), CB1 (1538 m), and CB2 (3219 m), displayed high microbial community similarity. This seemed consistent with the hypothesis that stable, core-dependent microbial communities, shaped by long-term geological and hydrological processes, might reveal past and present fluid–rock interactions and connectivity (Lever et al., 2013; Miettinen et al., 2018; Momper et al., 2017). In hydrologically connected areas such as fractures or permeable rock formations, fluid pathways serve as conduits for microbial dispersal and agents of environmental selection, driving community convergence (Bak et al., 2024). In terms of microbial functional potential, a distinct macro-geological pattern emerged: shallow samples (<3200 m) had a high-metabolism phenotype, whereas deep samples (>5000 m) revealed a low-metabolism. However, the metabolic activity of certain wells (e.g., ZG4, ZH1, ZG3) was decreased, likely because of physical isolation produced by reservoir heterogeneity or limits imposed by local geochemical circumstances (He et al., 2025b).

Table 2
Abundances and differences of dominant bacterial species among ecotypes.

Level	Species	A	B	C	D	*p*
Class	Bacilli	19.66	43.69	9.57	3.16	**0.002**
	Alphaproteobacteria	19.39	10.60	18.69	28.55	**0.027**†
	Actinobacteria	14.76	13.82	31.72	4.90	**0.039**†
	Gammaproteobacteria	16.09	11.02	9.94	10.00	0.570
	Betaproteobacteria	5.26	3.33	11.15	10.69	**0.008**
	Deinococci	3.56	3.52	5.83	4.55	0.655
	Clostridia	3.70	0.68	1.27	2.17	0.315
	Rubrobacteria	0.37	5.38	0.22	0.07	0.536
	Cytophagia	1.93	1.18	1.55	0.85	0.441
	Bacteroidia	1.64	0.42	2.47	3.63	0.277
	Flavobacteriia	0.81	1.10	0.59	3.27	**0.011**
	Deltaproteobacteria	1.16	0.12	0.29	3.12	**0.041**†
	Others	8.54	3.71	5.06	23.65	**0.000**
Genus	*Mesobacillus*	2.51	11.1	0.99	0.25	**0.011**
	Pseudoalteromonas	1.10	0.27	0.33	0.01	0.438
	Acinetobacter	5.21	2.09	6.42	0.98	0.433
	Metabacillus	0.71	10.02	0.66	0.07	**0.034**†
	Sphingomonas	2.92	1.29	2.14	3.15	0.401
	Kocuria	1.87	0.87	6.35	0.40	**0.040**†
	Thermus	1.86	0.41	3.15	4.42	0.268
	Rubrobacter	0.37	5.38	0.22	0.07	0.536
	Deinococcus	1.50	3.06	2.24	0.13	0.398
	Robertmurraya	0.41	5.18	0.30	0	**0.025**†
	Acidiphilium	0.07	0.03	0.18	12.60	**0.000**
	Burkholderia	1.23	0.26	2.75	4.36	**0.020**†
	Blastococcus	1.11	0.96	5.19	0.19	0.406
	Bradyrhizobium	1.09	0.20	5.12	0.79	**0.034**†
	Paracoccus	2.65	0.84	1.78	0.20	**0.000**

Notes: The numbers indicate the average species abundances within ecotypes ($n = 2$–5). p values indicate the differences among four ecotypes according to LSD test. Differences with q-value (Benjamini–Hochberg FDR-corrected) < 0.05 were considered statistically significant after correction. Significant differences ($p < 0.05$) that did not retain significance after FDR correction ($q > 0.05$) were indicated with superscript "†".

Based on bacterial community structure and predicted metabolic functions (PICRUSt2), the study wells were classified into four distinct ecotypes (Types A–D). While both Types A and B exhibited high intra-group interaction and metabolic activity, they possessed divergent ecological characteristics. Type A was distinguished by high bacterial diversity and a mixed trophic strategy, with genera like *Thermus*, *Bradyrhizobium*, and *Paracoccus*, all of which possessed broad organic matter degradation potential, showing greater abundances compared to Type B (Hao et al., 2004; Puri et al., 2022). Such features were most likely the results of forces such as geothermal activity and nitrogen restriction, of which contributed to a dynamic yet heterogenous fluid exchange network. In contrast, Type B was distinguished by copiotrophic bacteria such as *Mesobacillus* and *Metabacillus* and was formed predominantly by homogenous selection, indicating a steady hydraulic environment with inputs of easily degradable substrates (Li et al., 2019). Type C exhibited oligotrophic species composition and low metabolic activity. Although the community structure showed similarity to Type A, its low metabolic activity reflected strong physical isolation (Fig. 4). Type D harbored dominant microbial taxa that were rare in other ecotypes, indicating a unique and isolated niche. Although CHE4 and CB5 were located in different blocks with weak direct physical connectivity, the similar microbial composition between reservoir units containing CB5 and CHE4 reflected shared lithological and diagenetic evolution rather than current hydraulic connectivity.

Studies in sedimentary bedrock showed that microbial communities could exhibit convergence across geographically separated but lithologically analogous formations (He et al., 2025a; Ruiz-Blas et al., 2025). In this case, the community structure of Types A and C differed insignificantly different lithologies ($p < 0.05$), and the geographical isolation shaped distinct functions and possible connectivity. Meanwhile, both wells in Type D sharing similar carbonate lithology likely representing analogous geological environments did not represent active inter-well hydraulic connection, which was consistent with ecotype classification and reflected shared geological heritage rather than active fluid exchange. This convergence pattern in microbial communities was also known as parallel evolution, which meant isolated compartments experiencing comparable depositional and diagenetic histories might independently develop similar community structures through deterministic selection (Ruiz-Blas et al., 2025). However, results on the drivers of microbial community similarity indicated that hydraulic connectivity—rather than shared lithology alone—was the primary factor associated with microbial convergence within the same region (Fig. S4). Nevertheless, the convergent microbial signatures, such as rare biomarkers from

Table 3
Abundances and differences of dominant archaeal species among ecotypes.

Level	Species	Halophilic	Ammonia-oxidizing	Methanogenic	*p*
Class	Halobacteria	0.84	0.23	0.29	**0.002**
	Nitrososphaeria	0.15	0.71	0.08	**0.000**
	Methanobacteria	0.01	0.04	0.42	**0.000**
	Bathyarchaeia	0.00	0.01	0.11	**0.049**
	Thermoplasmata	0.00	0.00	0.05	**0.045**
	Others	0.00	0.01	0.05	**0.037**
Genus	*u_Nitrososphaeraceae*	0.11	0.59	0.06	**0.000**
	Halococcus	0.48	0.07	0.00	**0.006**
	Methanobacterium	0.01	0.02	0.25	**0.029**†
	u_Halobacterales	0.12	0.08	0.01	0.516
	Haloarcula	0.00	0.01	0.27	**0.034**†
	Halalkalicoccus	0.12	0.01	0.00	0.264
	u_Bathyarchaeia	0.00	0.01	0.11	**0.046**†
	Methanobrevibacter	0.00	0.01	0.10	**0.009**
	u_Nitrosopumilaceae	0.02	0.06	0.00	0.251
	u_Haloferacaceae	0.05	0.02	0.00	0.322
	Methanosphaera	0.00	0.00	0.07	0.180
	Halorussus	0.04	0.00	0.00	0.397
	Candidatus_Nitrososphaera	0.00	0.03	0.00	0.248
	Methanomassiliicoccus	0.00	0.00	0.04	**0.043**†
	Halogranum	0.00	0.02	0.00	0.545

Notes: The numbers indicate the average species abundances within ecotypes (n = 4–6). p values indicate the differences among four ecotypes according to LSD test. Differences with q-value (Benjamini–Hochberg FDR-corrected) < 0.05 were considered statistically significant after correction. Significant differences ($p < 0.05$) that did not retain significance after FDR correction ($q > 0.05$) were indicated with superscript "†".

these two wells, can provide a potential reference fingerprint for reservoir exploration despite their geographic and structural separation. Another possibility that might lead to community succession was contamination, which was correlated with exogenous DNA introduced by drilling fluids, generating spurious similarities among samples. However, the contamination controls, such as surface decontamination and comparison of drilling fluid records, significantly diminished the possibility of contamination. This was demonstrated by the absence of numerous aerobic microbial taxa—such as Burkholderiales, Sphingomonadaceae, and Sporichthyaceae—that are commonly found in drilling fluids in the core samples (Westmeijer et al., 2023; Zhang et al., 2020). Future studies require integrating microbial analysis with tracer testing and other methods to provide additional independent indicators of hydraulic connectivity for these undeveloped wells. In contrast to the ecotype wells discussed above, the three wells not assigned to core ecotypes (CB4, L4, ZG3) exhibited low bootstrap support (<50%) and varied classification under different community-functional weightings. These wells might be isolated by structural barriers and experienced distinct diagenetic histories, resulting in transitional or highly heterogeneous microbial assemblages where taxonomic and functional profiles were not tightly coupled. The instability of these wells in clustering suggested that they did not possess a strong, deterministic connectivity signal and therefore were appropriately excluded from the main ecotype framework (Felsenstein, 1985; Soltis and Soltis, 2003). Samples assigned to core ecotypes showed bootstrap supports ranging from 70% to 96%, indicating robust clustering. The equal weighting (0.5:0.5) remained justified for ecotype definition as it respected the potential decoupling of community structure and function, which was confirmed in subsurface and other environmental microbiomes (Chen et al., 2021; Louca et al., 2016). Data-driven weighting schemes or consensus clustering approaches could be employed in future studies to better resolve ambiguous wells.

Archaea, which served as sensitive markers for extreme conditions including high salinity and anaerobic conditions, showed community diversification as a result of long-term geological isolation and multi-scale rock-fluid-microbe interactions. Archaeal communities were known to exhibit a stronger distance-decay relationship than bacterial communities in subsurface oil reservoirs (Yun et al., 2021), and their distributions were governed by local geochemical gradients which could persist within hydraulically connected units due to incomplete mixing, spatially variable water–rock reactions, and microbial metabolic feedback (Gray and Engel, 2013; Randall, 2006). Therefore, archaeal distribution patterns could disclose local environmental variability and gave critical geochemical information for ecotype identification within connected units (Baker et al., 2020; Offre et al., 2013). In this study, archaeal communities formed distinct clusters based on physiological function (halophily, ammonia oxidation, methanogenesis), revealing microenvironmental variation within ecotypes. The co-occurrence of halophilic archaea (e.g., *Halococcus*, *Haloarcula*) in both Types A and B indicated a region-wide high-salinity selective pressure, consistent with the high-TDS hydrochemistry of these ecotypes (Fig. S10). Ammonia-oxidizing archaea (e.g., *Nitrosopumilaceae*) were more widely distributed across Types A, B, and C, pointing to a widespread nitrogen-enriched hydrological condition (Martens-Habbena and Qin, 2022). Wells like CB7, CB6, and ZG5, despite some extent of physical isolation, might have experienced similar low-nutrient or low-energy flux environments in the deep subsurface. The coexistence of diverse archaeal guilds (halophiles, ammonia oxidizers, methanogens) within Type A revealed geochemical gradient heterogeneity inside this ecotype. Notably, ZG1 in Type B exhibited a strong methanogenic signal, similar to CB5 and CHE4 in Type D, aligning with the elevated HCO_3^- concentration. This suggested the presence of a unique methanogenic niche within Type B, recording active deep subsurface carbon cycling (Osburn et al., 2014). The observed divergence between bacterial and archaeal patterns such as methanogenic archaea restricted to specific subzones within Type B, reflected domain-specific sensitivities to local geochemical gradients. Bacteria with broader metabolic versatility and shorter generation times could respond more rapidly to bulk fluid chemistry and dispersal, while archaea, particularly specialized halophiles and methanogens, often tracked narrower geochemical niches which varied within a connected unit. Thus, physical connectivity enabled mixing, but local geochemical heterogeneity preserved within the same connected network could still produce domain-specific distribution patterns (Ning et al., 2024). This

complexity underscored the necessity of integrating both bacterial and archaeal data for robust reservoir characterization.

4.2. Advantages of core-derived microorganisms as stable connectivity indicators

The inter-well stratigraphic correlation derived from high-resolution well-seismic calibration further supported the connectivity hypothesis based on microbial community similarity. Type A well group was situated within the same buried-hill structural trend, where substantial tectonic throw (up to 2200 m) and formation dip created fluid potential differences driving fluid mixing, leading to spatial heterogeneity of temperature and pressure. This heterogeneous paleo-hydrological environment provided diverse niches for microbial taxa in Type A responsible for degrading various organic compounds and promoted a stochastic community assembly process dominated by dispersal limitation (stochastic processes) (Zhou and Ning, 2017). In contrast, Type B group resided in a block with minor tectonic relief (about 600 m), providing a geological setting for stable fluid flow and strong homogeneous selection (deterministic processes). This environment favored the enrichment of a few copiotrophic bacteria like *Mesobacillus*, which efficiently utilized labile organic matter, leading to the lower bacterial diversity (Dini-Andreote et al., 2015). Deterministic and stochastic processes could coexist in the same hydrologic system, with the relative importances varying according to local hydrogeological conditions and nutrient availability (Zhou and Ning, 2017). In higher-velocity aquifers such as Type A, stochastic processes, especially dispersal, became more pronounced, whereas in low-velocity zones with stable nutrient supply (Type B), homogeneous selection dominated (Yan et al., 2020). However, the Es layer in which Types A and B were located consisted of shallow-lake bar-and-sill sand deposits, and each bar-and-sill sand body exhibited a lenticular shape in plane-view. Types A and B were located in separate lenticular bodies, separated by shallow-lake mudstone, which prevented them from being connected.

The sandbody pinch-out identified in the Type C group was a common heterogeneity issue in reservoir characterization that physically blocked lateral fluid migration, creating relatively isolated geological compartments (Zhang et al., 2021). The microbial community in Type C showed partial similarity to Type A but lower metabolic activity, possibly originating from shared sedimentary parent material followed by divergent community succession after physical isolation (Hanson et al., 2012). The alignment of microbial ecotype boundaries with independent seismic evidence of structural discontinuities (Types A and C) provided a necessary condition for inter-well connectivity, and further argued against the contamination as the primary driver for Types A, B, and C. However, the actual hydraulic connectivity at the well-pair level remained unclear, more independent methods such as inter-well tracer tests or pressure interference analysis were required to verify the inferred connectivity networks. Microbial community data, which integrated the cumulative effects of fluid exchange over geological time, provided a more sensitive indicator of connectivity. CB5, located in the Lower Cambrian ∈2z layer, was enriched with extremotolerant microbes like *Thermus* and *Acidiphilium*. This might indicate a unique geological fluid activity history for this reservoir unit, including deep hydrothermal fluid input and thermochemical degradation of organic matter (Jiao et al., 2022). This well and CHE4 from a different block might have intercepted the same set of depositional microfacies with distinctive lithological-geochemical attributes, which, while not necessarily hydraulically connected at present, shaped their shared and unique geochemical "fingerprint".

Mantel analysis indicated that hydrochemical factors selectively affected microbial community variation (Fig. 5(a)). TDS, Na^+, K^+, and HCO_3^-, acting as fundamental environmental stressors and key carbon sources, significantly influenced bacterial communities. In contrast, Ca^{2+}, Mg^{2+}, and SO_4^{2-} primarily affected archaeal community differentiation. The cell membrane structure and osmoregulation mechanisms differed substantially across bacterial taxa. Type B, especially CB6 and ZG5, with the highest TDS (>43000 mg/L) and Na^+ and K^+ concentrations (>14290 mg/L) possessed the high relative abundance of Bacilli (up to 63.7%), which was widely recognized for the capacity to synthesize compatible solutes and to maintain cellular turgor under hyperosmotic stress via K^+ uptake and osmolyte accumulation (Saum and Müller, 2007). This strongly supported the ecological adaptability of a few osmotolerant bacteria and significantly lower bacterial diversity in Type B under elevated salinity as a powerful environmental filter. The uniformly low SO_4^{2-} concentrations

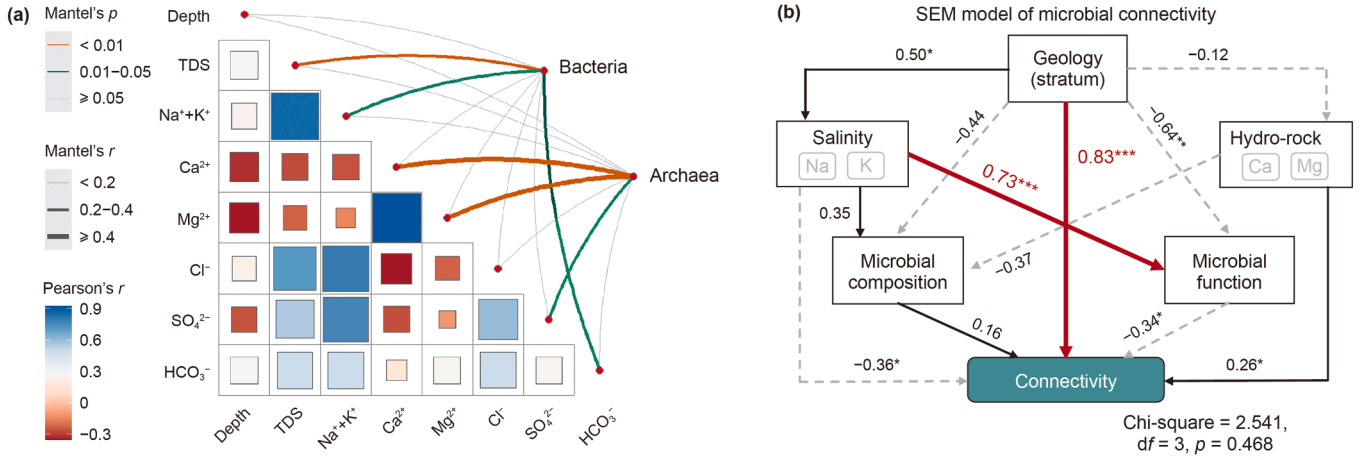


Fig. 5. The relationships between microbial communities and environmental conditions. (**a**) Effects of depth, mineralization, and ion concentrations on bacterial and archaeal communities revealed by Mantel analysis based on Pearson correlation. Bold and colored lines indicate significant correlations between environmental indicators and microbial communities: orange, $p < 0.01$; green, $0.01 < p < 0.05$. (**b**) The SEM model of stratum, hydrochemistry, microbial properties, and connectivity based on microbial ecotypes. Geology (stratum), stratigraphic depth; Salinity, the total concentrations of Na^+ and K^+; Hydro-rock, the total concentrations of Ca^{2+} and Mg^{2+}; Microbial composition, the ratio of copiotrophs to oligotrophs; Microbial function, the relative abundances of microbial metabolic pathways; Connectivity, indicated by microbial ecotype classification and confirmed by seismic data. All variables were normalized, and numbers indicate path coefficient: *, $p < 0.05$; **, $p < 0.01$; ***, $p < 0.001$.

(520–1291 mg/L) across all samples indicated near-complete sulfate reduction in this strongly reducing environment. The suppression of sulfate-reducing bacteria (SRBs) such as Desulfobulbaceae (relative abundance < 0.1%) reflected the depletion of electron acceptors, whereas methanogenic archaea (Methanobacterium) were enriched in zones with elevated HCO_3^- (>2500 mg/L), consistent with thermodynamic favorability of hydrogenotrophic methanogenesis under low SO_4^{2-} conditions (Pachiadaki et al., 2014; Sowakiewicz et al., 2024). Elevated HCO_3^- concentrations in some samples might indicate stronger evaporative concentration or specific organic matter degradation pathways, and also served as an important inorganic carbon source in the deep subsurface, directly participating in chemoautotrophic or mixotrophic metabolic strategies of various bacteria (Cheng et al., 2021). Local carbon source or sulfate availability, in addition to the overarching salinity selection, drove the differentiation of functional guilds such as methanogens or sulfate reducers, eventually forming a microenvironmental continuum containing geochemical gradients and metabolic functional zones. Furthermore, Ca^{2+} and Mg^{2+} concentrations were closely linked to the dissolution–precipitation equilibrium of carbonate (calcite, dolomite) and sulfate (gypsum) minerals, which were commonly combined with archaeal metabolic pathways such as methanogenesis and sulfate reduction (Baker et al., 2020). SEM further elucidated the correlations of connectivity based on microbial ecotype with stratum, hydrochemical environments, and community properties (Fig. 5(b)). We proposed that the geological structural background shaped the heterogeneity of microbial community structure and function through various mechanisms by altering the geochemical environment, ultimately reflecting the geological connectivity of the fracture network (Fig. 6). Several recent studies successfully used fluid-phase microbial communities to infer inter-well connectivity in fractured reservoirs and geothermal systems (Rizzo et al., 2020; Zhang et al., 2020). However, fluid-phase microbiomes were strongly influenced by short-term operational perturbations such as injection fluids, wellbore effects, and seasonal recharge, and might record connectivity over relatively short timescales. In contrast, core-derived microbial communities used in this study were more representative of long-term in-situ conditions as they were physically protected from rapid environmental fluctuations and integrated both dispersal and environmental selection over extended periods. Importantly, the long-term connectivity inferred from core-derived microbial analysis defined the intrinsic architecture of reservoirs, which fundamentally constrained short-term production dynamics. Unlike conventional tracers that captured operational connectivity over days to years, microbial signatures integrated fluid exchange over geological timescales, including fluid backflow or cross-formational recharge that were generally undetectable (Juliusson and Horne, 2013; Zhang et al., 2020). Thus, two wells with strong microbial similarity might exhibit transient "pressure isolation" due to near-wellbore damage, yet the underlying geological connectivity remained critical for understanding sweep efficiency and planning enhanced recovery strategies.

Consequently, even if two wells (e.g., ZG1 in Type B and CB5 in Type D) shared similar geochemical backgrounds due to analogous sedimentary–diagenetic histories, subtle differences in their micro-scale water–rock interaction processes were amplified by microbial communities. This was manifested as discrimination across hundreds to thousands of microbial taxonomic units or functional genes, offering discriminatory capacity significantly surpassing conventional hydrochemical and macroscopic well-seismic data (Juliusson and Horne, 2013; Vigneron et al., 2017). Wells separated by geological discontinuities might have comparable microbiological fingerprints due to deep paleo-hydrological linkages or homologous geochemical processes, reflecting long-term integration of geological and chemical data (Thompson et al., 2021). Meanwhile, the per-sample cost for 16S amplicon sequencing was substantially lower than that of conventional single-well tracer tests, especially when samples were processed in large batches. In this study, the sample size of 16 wells, while comparable to or exceeding many subsurface microbial studies, was modest for fully characterizing the heterogeneity of a complex buried-hill reservoir system. Several factors partially mitigated

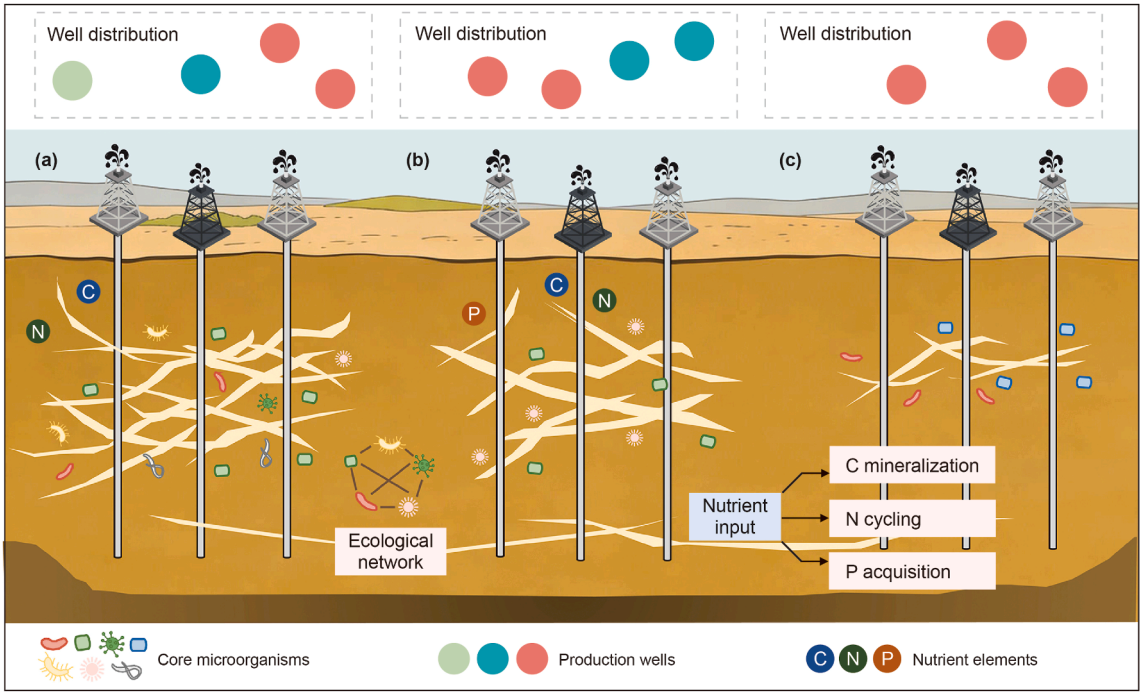


Fig. 6. Conceptual diagram of hypothesized fracture connectivity patterns for microbial ecotypes A, B, and C.

this concern: (1) sampled wells spanned the major structural domains (Type A: tectonically active block; Type B: stable block; Type C: pinch-out zone; and Type D: distinct sedimentary-diagenetic setting), capturing key geological variability; (2) bootstrap resampling (1000 iterations) yielded >64% assignment confidence for all core ecotype wells. Nonetheless, future studies incorporating larger sample sets and multi-well pads were necessary to validate the proposed ecotype framework and to establish its broader applicability across different reservoir types. Core-derived microbial data might thus illuminate not only the hydraulic connection structure in the deep subsurface, but also act as biomarkers signaling microenvironmental zonation within linked units, providing insight on the underlying biogeochemical processes. This strategy of integrating microbial communities with geochemical data to establish a composite microbial indicator system held the potential for more accurate reconstruction of long-term subsurface hydrogeological history and definition of fundamental reservoir architecture, thus offering a novel approach grounded in ecological principles for optimizing well placement and enhancing hydrocarbon recovery.

4.3. Potential applications and current limitations

The inter-well connectivity inferred from core-derived microbial ecotypes offered potential value for reservoir development planning. However, the correlation between microbial community similarity and seismically defined connectivity is not universal for all reservoir types. Strong environmental selection and flow-regime-dependent stochastic assembly can decouple microbial similarity from physical connectivity (Yan et al., 2020; Zhang et al., 2022). It indicated that the approach may not be directly transferable to systems with extreme geochemical gradients or highly heterogeneous fluid mixing though performing well in high-permeability buried-hill reservoir. The method was developed for and tested only in high-permeability buried-hill fractured reservoirs where archived core samples were available and dynamic data were limited during exploration or early development stages. The applicability to other reservoir types such as tight sandstones, carbonates, and shale oil systems required independent validation, and it was less applicable in settings where indigenous microbial communities have been altered by drilling fluids, biocides, or extensive production operations. Meanwhile, it should not be generalized to tight reservoirs, shale oil, or other low-permeability systems before independent validation. The seismic and well-log evidence supported structural continuity satisfying a necessary condition for connectivity, while did not prove dynamic connectivity. Unresolved heterogeneities such as sub-seismic faults or localized permeability variations might still exist within an ecotype. Therefore, validation with independent methods, such as tracer tests or pressure interference analysis on a subset of well pairs, is recommended to be combined with the proposed microbial approach before operational decisions. We emphasize that this approach remains at a research stage and requires further validation across diverse geological settings and reservoir types before routine field application. Future work should focus on prospective blind validation studies and the development of standardized analytical protocols to facilitate broader industry adoption.

5. Conclusions

This study systematically investigated inter-well connectivity in the buried-hill reservoir of the Jiyang Depression by integrating microbial community analysis with geochemical characterization of core samples. First, in situ microbial communities preserved within cores were confirmed as reliable and sensitive biological indicators of subsurface connectivity. The microbial composition and distribution reflected long-term adaptation to prevailing geochemical and hydrogeological conditions and categorized the investigated wells into four distinct ecotypes (Types A–D) based on metrics of community similarity, phylogenetic relatedness, and metabolic functions. While both Type A and Type B exhibited strong intra-group connectivity, they represented divergent metabolic regimes (mixotrophic and copiotrophic), suggesting different subsurface fluid networks and nutrient availability. In contrast, Type C displayed poor connectivity due to physical isolation resulting from reservoir pinch-out, whereas Type D reflected a specialized sedimentary–diagenetic niche characterized by a distinct taxonomic and functional profile. This ecotype classification was corroborated by a structural equation model and well-seismic stratigraphic correlation, confirming the alignment between microbial data and the macroscopic geological framework. Furthermore, microbial data offered high-throughput and detailed community information, enabling fine-scale discrimination of reservoir units sharing similar geological origins but hydraulically isolated. Taxa with specific metabolic functions could reveal microenvironmental heterogeneity within ecotypes, which were hypothesized to reflect connectivity patterns, thereby assisting in reconstructing geochemical processes associated with fluid migration and elemental cycling. In summary, core-derived microbial communities served as spatially resolved “biological fingerprints” elucidating both inter-well connectivity and internal heterogeneity in complex fractured reservoirs, overcoming the limitations of conventional physicochemical methods. Future studies could integrate microbiome data with production performance metrics and artificial intelligence-driven modeling to advance towards more precise reservoir characterization and management.

CRediT authorship contribution statement

Guang-Yuan Sun: Writing – original draft, Investigation, Data curation. **Shu-Jie Xiao:** Writing – original draft, Visualization, Validation, Software, Methodology, Investigation, Formal analysis, Data curation, Conceptualization. **Yong-Ting Song:** Supervision, Resources, Conceptualization. **Yang Gao:** Visualization, Methodology, Formal analysis. **Ai-Min Jin:** Writing – review & editing, Project administration, Funding acquisition. **Zhang-Hua Lou:** Writing – review & editing, Project administration, Funding acquisition.

Declaration of competing interest

The authors declare that they have no known competing financial interests or personal relationships that could have appeared to influence the work reported in this paper.

Acknowledgements

This work was supported by the National Science and Technology Major Project “Patterns of Hydrocarbon Enrichment and Exploration Technologies for New Areas in the Bohai Bay Super Basin” (No. 2024ZD1400100).

Supplementary data

Supplementary data to this article can be found online at https://doi.org/10.1016/j.petsci.2026.07.005.

References

Bak, F., Keuschnig, C., Nybroe, O., Aamand, J., Jrgensen, P.R., Nicolaisen, M.H., Vogel, T.M., Larose, C., 2024. Microbial life in preferential flow paths in subsurface clayey till revealed by metataxonomy and metagenomics. BMC Microbiol. 24, 296. https://doi.org/10.1186/s12866-024-03432-z.

Baker, B.J., Anda, V.D., Seitz, K.W., Dombrowski, N., Lloyd, K.G., 2020. Diversity, ecology and evolution of Archaea. Nat. Microbiol. 5, 1–14. https://doi.org/10.1038/s41564-020-0715-z.

Caicedo, H.H., Hashimoto, D.A., Caicedo, J.C., Pentland, A., Pisano, G.P., 2020. Overcoming barriers to early disease intervention. Nat. Biotechnol. 38, 669–673. https://doi.org/10.1038/s41587-020-0550-z.

Campos, A.F., Cassella, A.R., Cassella, R.J., 2020. Microwave-assisted extraction of chloride followed by ion chromatography as an alternative to the ASTM D6470 method for the determination of crude oil salinity. Energy Fuels 34, 6844–6850. https://doi.org/10.1021/acs.energyfuels.0c00425.

Chen, Y., Liu, F., Kang, L., Zhang, D., Kou, D., Mao, C., Qin, S., Zhang, Q., Yang, Y., 2021. Large-scale evidence for microbial response and associated carbon release after permafrost thaw. Glob. Change Biol. 27, 3218–3229. https://doi.org/10.1111/gcb.15487.

Chen, S.-C., Li, X.-M., Battisti, N., Guan, G., Montoya, M.A., Osvatic, J., Pjevac, P., Pollak, S., Richter, A., Schintlmeister, A., Wanek, W., Mussmann, M., Loy, A., 2025. Microbial iron oxide respiration coupled to sulfide oxidation. Nature 646, 925–933. https://doi.org/10.1038/s41586-025-09467-0.

Cheng, A.-Q., Kang, W.-H., Li, W., Yu, L.-J., 2021. Research progress on autotrophic carbon fixation processes and mechanisms driven by soil microorganisms in karst regions. Acta Microbiol. Sin. 61 (6), 1525–1535. https://doi.org/10.13343/j.cnki.wsxb.20210130 (in Chinese).

Cui, B., Liu, X., Yang, Q., Li, J., Zhou, X., Peng, Y., 2017. Achieving partial denitrification through control of biofilm structure during biofilm growth in denitrifying biofilter. Bioresour. Technol. 238, 223–231. https://doi.org/10.1016/j.biortech.2017.04.034.

Dahlke, H.E., Williamson, A.G., Georgakakos, C., Leung, S., Sharma, A.N., Lyon, S.W., Walter, M.T., 2015. Using concurrent DNA tracer injections to infer glacial flow pathways. Hydrol. Process. 29, 5257–5274. https://doi.org/10.1002/hyp.10679.

Deng, Y., Jiang, Y.H., Yang, Y., He, Z., Luo, F., Zhou, J., 2012. Molecular ecological network analyses. BMC Bioinf. 13, 113. https://doi.org/10.1186/1471-2105-13-113.

Dini-Andreote, F., Stegen, J.C., van Elsas, J.D., Salles, J.F., 2015. Disentangling mechanisms that mediate the balance between stochastic and deterministic processes in microbial succession. Proc. Natl. Acad. Sci. 112. https://doi.org/10.1073/pnas.1414261112.

Felsenstein, J., 1985. Confidence limits on phylogenies: An approach using the bootstrap. Evolution 39, 783–791. https://10.1111/j.1558-5646.1985.tb00420.x.

Feng, K., Zhang, Z., Cai, W., Liu, W., Xu, M., Yin, H., Wang, A., He, Z., Deng, Y., 2017. Biodiversity and species competition regulate the resilience of microbial biofilm community. Mol. Ecol. 26, 6170–6182. https://doi.org/10.1111/mec.14356.

Fierer, N., Bradford, M.A., Jackson, R.B., 2007. Toward an ecological classification of soil bacteria. Ecology 88, 1354–1364. https://doi.org/10.1890/05-1839.

Finn, D., Kopittke, P.M., Dennis, P.G., Dalal, R.C., 2017. Microbial energy and matter transformation in agricultural soils. Soil Biol. Biochem. 111, 176–192. https://doi.org/10.1016/j.soilbio.2017.04.010.

Fredrickson, J.K., Balkwill, D.L., 2006. Geomicrobial processes and biodiversity in the deep terrestrial subsurface. Geomicrobiol. J. 23, 345–356. https://doi.org/10.1080/01490450600875571.

Gray, C.J., Engel, A.S., 2013. Microbial diversity and impact on carbonate geochemistry across a changing geochemical gradient in a karst aquifer. ISME J. 7, 325–337. https://10.1038/ismej.2012.105.

Hanson, C.A., Fuhrman, J.A., Horner-Devine, M.C., Martiny, J.B.H., 2012. Beyond biogeographic patterns: Processes shaping the microbial landscape. Nat. Rev. Microbiol. 10, 497–506. https://doi.org/10.1038/nrmicro2795.

Hao, R., Lu, A., Wang, G., 2004. Crude-oil-degrading thermophilic bacterium isolated from an oil field. Can. J. Microbiol. 50 (3), 175. https://doi.org/10.1139/w03-116.

He, X., Wang, R., Goll, D.S., Augusto, L., Nunan, N., Farnon Ellwood, M.D., Gao, Q., Huang, J., Qian, S., Zhang, Y., Shu, Z., Li, B., Chu, C., 2025a. Bedrock modulates the elevational patterns of soil microbial communities. Geoderma 453, 117136. https://doi.org/10.1016/j.geoderma.2024.117136.

He, Y., Liu, K., Huang, T., Wang, W., Zhang, X., Bai, L., Zhang, J., Huang, H., 2025b. Microbial community assembly and functional adaptation of urease-producing bacteria in oil reservoirs: Driven by phase heterogeneity and selective enrichment. J. Environ. Chem. Eng. 13. https://doi.org/10.1016/j.jece.2025.120521.

Hinrichs, K.U., Inagaki, F., 2012. Downsizing the deep biosphere. Science 338, 204–205. https://doi.org/10.1126/science.1229296.

Jiao, J.Y., Lian, Z.H., Li, M.M., Salam, N., Zhou, E.M., Liu, L., Ming, H., Nie, G., Shu, W., Zhao, G., 2022. Comparative genomic analysis of *Thermus* provides insights into the evolutionary history of an incomplete denitrification pathway. mLife 1 (2), 198–209. https://doi.org/10.1002/mlf2.12009.

Juliusson, E., Horne, R.N., 2013. Characterization of fractured reservoirs using tracer and flow-rate data. Water Resour. Res. 49, 2327–2342. https://doi.org/10.1002/wrcr.20220.

Kallmeyer, J., Pockalny, R., Adhikari, R.R., Smith, D.C., D'Hondt, S., 2012. Global distribution of microbial abundance and biomass in subseafloor sediment. Proc. Natl. Acad. Sci. 109, 16213–16216. https://doi.org/10.1073/pnas.1203849109.

Kieft, T.L., Phelps, T.J., Fredrickson, J.K., 2008. Drilling, coring, and sampling subsurface environments. ChemInform 39. https://doi.org/10.1002/chin.200811273.

Lehman, R.M., Roberto, F.F., Earley, D., Bruhn, D.F., Brink, S.E., O'Connell, S.P., Delwiche, M.E., Colwell, F.S., 2001. Attached and unattached bacterial communities in a 120-meter corehole in an acidic, crystalline rock aquifer. Appl. Environ. Microbiol. 67 (5). https://doi.org/10.1128/AEM.67.5.2095-2106.

Lever, M.A., Alperin, M., Engelen, B., Inagaki, F., Teske, A., 2006. Trends in basalt and sediment core contamination during IODP expedition 301. Geomicrobiol. J. 23, 517–530. https://10.1080/01490450600897245.

Lever, M.A., Rouxel, O., Alt, J.C., Shimizu, N., Ono, S., Coggon, R.M., Shanks, W.C., Lapham, L., Elvert, M., Prieto-Mollar, X., 2013. Evidence for microbial carbon and sulfur cycling in deeply buried ridge flank basalt. Science 339, 1305–1308. https://doi.org/10.1126/science.1229240.

Li, W., Wei, F., Chen, X., Yu, Z., Zhou, Z., Zhang, Y., Ma, S., Meng, Q., Yang, C., 2025. Dynamic calculation method of interwell connectivity based on the attention mechanism. Energy Sci. Eng. 13, 1807–1818. https://doi.org/10.1002/ese3.70011.

Li, X.M., Chen, Q.L., He, C., Shi, Q., Chen, S.C., Reid, B.J., Zhu, Y.G., Sun, G.X., 2019. Organic carbon amendments affect the chemodiversity of soil dissolved organic matter and its associations with soil microbial communities. Environ. Sci. Technol. 53, 50–59. https://doi.org/10.1021/acs.est.8b04673.

Ligtenberg, J.H., 2005. Detection of fluid migration pathways in seismic data: Implications for fault seal analysis. Basin Res. 17, 141–153. https://doi.org/10.1111/j.1365-2117.2005.00258.x.

Louca, S., Parfrey, L.W., Doebeli, M., 2016. Decoupling function and taxonomy in the global ocean microbiome. Science 353, 1272–1277. https://10.1126/science.aaf450.

Magnabosco, C., Lin, L.H., Dong, H., Bomberg, M., Ghiorse, W., Stan-Lotter, H., Pedersen, K., Kieft, T.L., Heerden, E.V., Onstott, T.C., 2018. The biomass and biodiversity of the continental subsurface. Nat. Geosci. 11, 707–717. https://doi.org/10.1038/s41561-018-0221-6.

Martens-Habbena, W., Qin, W., 2022. Archaeal nitrification without oxygen. Science 375. https://doi.org/10.1126/science.abn0373.

Miall, A.D., 1995. Whither stratigraphy? Sediment. Geol. 100, 5–20. https://doi.org/10.1016/0037-0738(95)00100-X.

Miettinen, H., Bomberg, M., Vikman, M., 2018. Acetate activates deep subsurface fracture fluid microbial communities in Olkiluoto, Finland. Geosciences 8 (11), 399. https://doi.org/10.3390/geosciences8110399.

Mitchum, R.M., Vail, P.R., 1977. Seismic tratigraphy and global changes of sea level; Part 7, seismic stratigraphic interpretation procedure. In: Payton, C.E. (Ed.), Seismic Stratigraphy—Applications to Hydrocarbon Exploration. https://doi.org/10.1029/2002GL015986.

Momper, L., Kiel Reese, B., Zinke, L., Wanger, G., Osburn, M.R., Moser, D., Amend, J.P., 2017. Major phylum-level differences between porefluid and host rock bacterial communities in the terrestrial deep subsurface. Environ. Microbiol. Rep. 9, 501–511. https://doi.org/10.1111/1758-2229.12563.

Ning, D., Wang, Y., Fan, Y., Wang, J., Van Nostrand, J.D., Wu, L., Zhang, P., Curtis, D.J., Tian, R., Lui, L., 2024. Environmental stress mediates groundwater microbial community assembly. Nat. Microbiol. 9, 490–501. https://doi.org/10.1038/s41564-023-01573-x.

Offre, P., Spang, A., Schleper, C., 2013. Archaea in biogeochemical cycles. Annu. Rev. Microbiol. 67, 437–457. https://doi.org/10.1146/annurev-micro-092412-155614.

Okoro, C., Smith, S., Chiejina, L., Lumactud, R., An, D., Park, H.S., Voordouw, J., Lomans, B.P., Voordouw, G., 2014. Comparison of microbial communities involved in souring and corrosion in offshore and onshore oil production facilities in Nigeria. J. Ind. Microbiol. Biotechnol. 41, 665–678. https://doi.org/10.1007/s10295-014-1401-z.

Osburn, M.R., Larowe, D.E., Momper, L.M., Amend, J.P., 2014. Chemolithotrophy in the continental deep subsurface: Sanford Underground Research Facility (SURF), USA. Front. Microbiol. 5, 610. https://doi.org/10.3389/fmicb.2014.00610.

Pachiadaki, M.G., Yakimov, M.M., Lacono, V., Leadbetter, E., Edgcomb, V., 2014. Unveiling microbial activities along the halocline of Thetis, a deep-sea hypersaline anoxic basin. ISME J. 8, 2478–2489. https://doi.org/10.1038/ismej.2014.100.

Petro, C., Starnawski, P., Schramm, A., Kjeldsen, K.U., 2017. Microbial community assembly in marine sediments. Aquat. Microb. Ecol. 79, 177–195. https://doi.org/10.3354/ame01826.

Puri, A., Bajaj, A., Singh, Y., Lal, R., 2022. Harnessing taxonomically diverse and metabolically versatile genus Paracoccus for bioplastic synthesis and xenobiotic biodegradation. J. Appl. Microbiol. 132, 4208–4224. https://doi.org/10.1111/jam.15530.

Randall, K.W., 2006. Assessing the Potential Impact of Microbes in the Edwards and Trinity Aquifers of Central Texas. M.S. Thesis. Louisiana State University and Agricultural and Mechanical College. https://10.31390/gradschool_theses.1110.

Rizzo, P., Petrella, E., Bucci, A., Salvioli-Mariani, E., Celico, F., 2020. Studying hydraulic interconnections in low-permeability media by using bacterial communities as natural tracers. Water 12, 1795. https://doi.org/10.3390/w12061795.

Ruiz-Blas, F., Friese, A., Bartholomäus, A., Henny, C., Russell, J.M., Kallmeyer, J., Vuillemin, A., 2025. The deep subsurface biosphere and its substrates along a

one-million-year ferruginous lake archive. Microb. Ecol. 88, 58. https://doi.org/10.1007/s00248-025-02559-4.
Saum, S.H., Müller, V., 2007. Salinity-dependent switching of osmolyte strategies in a moderately halophilic bacterium: Glutamate induces proline biosynthesis in *Halobacillus halophilus*. J. Bacteriol. 189, 6968–6975. https://doi.org/10.1128/jb.00775-07.
Shokralla, S., Spall, J.L., Gibson, J.F., Hajibabaei, M., 2012. Next-generation sequencing technologies for environmental DNA research. Mol. Ecol. 21, 1794–1805. https://doi.org/10.1111/j.1365-294X.2012.05538.x.
Sinclair, J.L., Ghiorse, W.C., 1989. Distribution of aerobic bacteria, protozoa, algae, and fungi in deep subsurface sediments. Geomicrobiol. J. 7, 15–31. https://doi.org/10.1080/01490458909377847.
Soltis, P.S., Soltis, D.E., 2003. Applying the bootstrap in phylogeny reconstruction. Stat. Sci. 18, 256–267. https://10.1214/ss/1063994980.
Sowakiewicz, M., Goraj, W., Segit, T., Wtor, K., Dobrzyński, D., 2024. Hydrochemical gradients driving extremophile distribution in saline and brine groundwater of southern Poland. Environ. Microbiol. Rep. 16, 17. https://doi.org/10.1111/1758-2229.70030.
Stegen, J.C., Lin, X., Fredrickson, J.K., Chen, X., Kennedy, D.W., Murray, C.J., Rockhold, M.L., Konopka, A., 2013. Quantifying community assembly processes and identifying features that impose them. ISME J. 7, 2069–2079. https://doi.org/10.1038/ismej.2013.93.
Thompson, T.P., Kelly, S.A., Skvortsov, T., Plunkett, G., Ruffell, A., Hallsworth, J.E., Hopps, J., Gilmore, B.F., 2021. Microbiology of a NaCl stalactite 'salticle' in Triassic halite. Environ. Microbiol. 23, 3881–3895. https://doi.org/10.1111/1462-2920.15524.
Vigneron, A., Alsop, E.B., Lomans, B.P., Kyrpides, N.C., Head, I.M., Tsesmetzis, N., 2017. Succession in the petroleum reservoir microbiome through an oil field production lifecycle. ISME J. 11, 2141–2154. https://doi.org/10.1038/ismej.2017.78.
Westmeijer, G., Escudero, C., Bergin, C., Turner, S., Sthle, M., Mehrshad, M., Leroy, P., Buck, M., López-Hernández, P., Kallmeyer, J., 2023. Continental scientific drilling and microbiology: (extremely) low biomass in crystalline bedrock of central Sweden. Biogeosciences 21, 591–604. https://10.5194/bg-2023-147.
Wu, X., Zhu, J., He, H., 2025. Crustal faulting drives biological redox cycling in the deep subsurface. Sci. Adv. 11 (29). https://doi.org/10.1126/sciadv.adx5372.
Xiao, S., Gao, J., Wang, Q., Huang, Z., Zhuang, G., 2024. SOC bioavailability significantly correlated with the microbial activity mediated by size fractionation and soil morphology in agricultural ecosystems. Environ. Int. 186, 108588. https://doi.org/10.1016/j.envint.2024.108588.
Yan, L., Herrmann, M., Kampe, B., Lehmann, R., Totsche, K.U., Küsel, K., 2020. Environmental selection shapes the formation of near-surface groundwater microbiomes. Water Res. 170, 115341. https://doi.org/10.1016/j.watres.2019.115341.
Yang, Y., Dai, Y., Wu, Z., Xie, S., Liu, Y., 2016. Temporal and spatial dynamics of archaeal communities in two freshwater lakes at different trophic status. Front. Microbiol. 7, 451. https://doi.org/10.3389/fmicb.2016.00451.
Yousefi, S.H., Rashidi, F., Sharifi, M., Soroush, M., 2018. On determination of interwell connectivity under immiscible gas injection process: Modified capacitance-resistance model. Can. J. Chem. Eng. 97, 1008–1021. https://doi.org/10.1002/cjce.23294.
Yun, Y., Gui, Z., Chen, Y., Tian, X., Gao, P., Li, G., Ma, T., 2021. Disentangling the distinct mechanisms shaping the subsurface oil reservoir bacterial and archaeal communities across northern China. Sci. Total Environ. 789, 148074. https://doi.org/10.1016/j.scitotenv.2021.148074.
Zhang, X.-T., Li, X.-P., Xuan, C.-J., Du, J.-Y., Ding, L., Li, Z.-G., Chen, W.-T., 2021. Exploration practices and future directions for lithologic reservoirs in non-hydrocarbon source rock formations within the shallow waters of the eastern South China Sea. Acta Petroleum Sinica 42 (6), 695–707. https://doi.org/10.7623/syxb202106001 (in Chinese).
Zhang, Y., Dekas, A.E., Hawkins, A.J., Parada, A.E., Gorbatenko, O., Li, K., Horne, R.N., 2020. Microbial community composition in deep-subsurface reservoir fluids reveals natural interwell connectivity. Water Resour. Res. 56 (2). https://doi.org/10.1029/2019wr025916.
Zhang, Y., Dekas, A.E., Hawkins, A.J., Primo, J.C., Gorbatenko, O., Horne, R.N., 2022. Comparison of microbial profiling and tracer testing for the characterization of injector-producer interwell connectivities. Water 14 (18), 2921. https://doi.org/10.3390/w14182921.
Zhou, J.Z., Ning, D.L., 2017. Stochastic community assembly: Does it matter in microbial ecology? Microbiol. Mol. Biol. Rev. 81 (4). https://doi.org/10.1128/MMBR.00002-17.